THE PENNSYLVANIA STATE UNIVERSITY
SCHREYER HONORS COLLEGE

DEPARTMENT OF MECHANICAL ENGINEERING

A NOVEL COMPLIANT MECHANICAL DISPLACEMENT AMPLIFIER

BRIAN DANIEL CHILSON
SPRING 2018

A thesis
submitted in partial fulfillment
of the requirements
for a baccalaureate degree
in MECHANICAL ENGINEERING
with honors in MECHANICAL ENGINEERING

Reviewed and approved* by the following:

Aman Haque
Professor of Mechanical Engineering
Thesis Supervisor

Jaqueline O'Connor
Assistant Professor of Mechanical Engineering
Honors Advisor

* Signatures are on file in the Schreyer Honors College.

ABSTRACT

Mechanical displacement amplification technology has a plethora of applications from large-scale gear trains and levers to micromechanical piezo-actuators and even variable braille displays. These are devices that accept an input displacement and, through a combination of connective linkages, amplify said displacement with the corresponding minimization of force output consistent with energy conservation. Common applications for micromechanical displacement amplifiers (MDA) include energy generation from ambient kinetic sources such as vibration, wave motion, or wind. Piezo-materials, which respond to an induced voltage with small elongations, are commonly coupled with MDA technology to amplify the output displacement from the piezo-material and develop more viable piezo-actuators. This thesis proposes a novel small-scale compliant mechanical displacement amplification mechanism designed for high force-input ambient kinetic energy generation.

The 15.72-gram mechanical displacement amplifier proposed herein exhibits an amplification ratio of 28.68 with a corresponding force transmission of 2.44% in response to an 800-Newton force input. It demonstrates a resonance frequency of 100.2 Hz. It is designed to be constructed from hot isostatically pressed titanium alloy Ti-6Al-4V due to this material's high-strength, low-density, magnetic properties, and conductivity to flexure hinges. The mechanism is compliant and relies on flexural hinges rather than sliding joints in its connectivity; this enhances durability, reduces maintenance, and permits manufacturing via additive manufacturing. Finally, this thesis suggests coupling electromagnetic energy generation technology with the MDA for the construction of a high force input, low-displacement ambient kinetic energy generator.

TABLE OF CONTENTS

LIST OF FIGURES

LIST OF TABLES

ACKNOWLEDGEMENTS

I would like to thank Dr. Jacqueline O'Connor for being a great advisor, mentor, and professor throughout my undergraduate experience in Mechanical Engineering at Penn State. I would also like to thank Dr. Aman Haque for his assistance, advice, and occasional inspiration during the development of this research project. He introduced me to the very fascinating ideas of ambient kinetic energy harvesting and mechanical displacement amplification. Because of his influence, the process of researching, designing, iterating, and writing for this thesis has been a very interesting and passion-inducing pursuit.

I would also like to thank Francisco Peralta, my friend from Berkeley, California. Our lengthy talks about the functions and shortfalls of prosthetic limbs in the context of mechanical engineering inspired my interest in energy generation from ambient kinetics sources such as the human gait.

Finally, I would like to thank my parents. The incredibly positive influence they have had on me throughout my childhood is the reason why I am at Penn State Schreyer studying something challenging like Mechanical Engineering. I cannot imagine where I'd be without them.

Chapter 1

Introduction

The purpose of this thesis is to propose a novel mechanical displacement amplification device, designed to absorb axial displacement and amplify said displacement utilizing a series of flexing levers and buckling beams. Finite Element Analysis was used to extensively to model a series of iterations on the MDA structure to analyze how to optimize displacement amplification and while maintaining durability and force transmission in a compliant micromechanical device. The MDA is designed for the purpose of high force input ambient kinetic energy generation; a variety of characteristics were maintained in the design of the device in order to accomplish these aims.

The MDA is designed to respond to a force input of 800 Newtons with a deformation on the scale of micrometers. This response is conducive to energy generation within high force input conditions such as the human step. The device is designed to be small and lightweight so that it can be used in small-scale applications without being cumbersome.

The device is designed to operate effectively over millions of cycles. At no volume element in the mechanism does the maximum Von Mises stress exceed the endurance limit of hot isostatically pressed titanium alloy Ti-6Al-4V. A larger amplification ratio could be achieved if the flexure hinges and buckling beam were made thinner; however, this would compromise the durability of the mechanism by inducing greater fatigue stress.

The mechanical displacement amplifier is a compliant mechanism; that is, it is constructed from one stock of material. Rotating and sliding parts require lubrication and can introduce large frictional damping if tainted by dirt or dust. Flexure hinges, on the other hand, smoothly and predictably rotate over millions of cycles. Considering recent technological advancements in additive manufacturing and electron beam melting, compliant mechanisms are the dominant style of displacement amplification. The usage of flexure hinges instead of sliding joints and pinions improves durability, predictability, and manufacturability.

The mechanism should deform elastically with minimal mechanical damping. This will maximize force transmission and amplification ratio. This is the reasoning behind displacement amplification which relies so heavily on the flexure of metal.

The following sections of this thesis will introduce the theoretical displacement amplification design and the model design. It will thoroughly expound upon the design choices and the process that led to the dimensional parameters associated with the force input, flexure hinges, buckling structures, etc. By the conclusion, the reader should have a detailed idea of the concepts behind the design and the rationale behind each dimensional choice.

Chapter 2

Literature Review

2.1. Mechanical Displacement Amplification

In the pursuit of deriving energy from ambient vibration and impulse, limited input deformation poses a significant impediment to power generation. For many applications in which energy is to be derived from the step of a prosthetic, the vibration of a machine, or the impression of an electronic button, the allowable input displacement is simply too small to directly develop viable power output. Mechanical displacement amplification (MDA) utilizes linkage mechanisms in a specific geometry to amplify the magnitude of an input displacement, thereby addressing the shortfalls of small-scale energy generation.

Mechanical input amplification is not new technology. Many have employed this technology, probably dating back to the first ape who realized he or she could lift a rock by wedging a stick beneath to act as a lever and amplify the force input. From the gear train of an automobile's transmission to the amplification of stress in a micro tensile-test structure, many applications utilize displacement amplification. This research endeavor seeks a novel displacement amplifier, and so it is useful to consider the displacement amplification mechanisms preceding this research. A multitude of specific connective arrangements between rigid linkages offer some sort of enhanced displacement; as per the law of conservation of energy each arrangement reduces the force output in an amount at least proportional to the enhancement in displacement, as demonstrated by equation 1:

$$F_{in} * \delta_{in} = F_{out} * \delta_{out} \quad (1)$$

This relationship represents the ideal force reduction; oftentimes inefficiencies in the linkage connections reduce force output even further than this limit. One must primarily consider the transmission of force and the amplification of displacement in the analysis of the following displacement amplification mechanisms.

2.1.1. Resonant versus Non-Resonant Mechanical Amplifiers

One may largely categorize displacement amplifiers as either resonant or non-resonant. Resonant amplifiers are non-rigid bodies specifically designed to resonate at the operating frequency of their application, thus exhibiting a buildup of oscillation amplitude over time. Resonant operation piezomotors are highly efficient in both displacement and force output; however, their frequency operation bandwidth is severely limited and hinders displacement amplification to applications in which the input vibration frequency is constant and known.

To the contrary, non-resonant mechanical amplifiers demonstrate lower efficiency but exhibit greater flexibility in potential applications since they amplify displacement across a range of frequency bandwidths. Since this research focuses on power generation from a non-constant source of force input, non-resonant amplifiers will be the focus [1].

2.1.2. Fundamental Displacement Principles

The plethora of existing MDA configurations depend on a few fundamental geometric principles. It is important to understand these constitutional mathematical foundations so often employed by various displacement amplification mechanisms.

The first fundamental geometric mechanism is Pythagorean displacement amplification. According to the Pythagorean Theorem, the sum of the squares of the legs of a right triangle is equal to the square of the hypotenuse. So, if the length of the hypotenuse is constant, a reduction in the length of the longer leg of the triangle results in an amplified increase in the length of the shorter leg. Figure 1 illustrates this simple principle. Equation 2 expresses this relationship [2]:

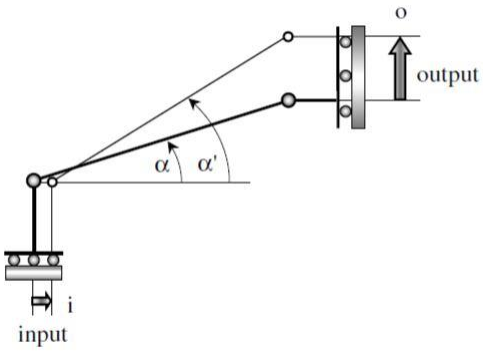

Figure 1: Pythagorean Displacement Amplification Principle [2]

$$\delta_{out} = \sqrt{l^2 (\sin\alpha)^2 + \delta_{in}(2l\cos\alpha - \delta_{in})} - l\sin\alpha \quad (2)$$

Mechanical displacement amplification widely utilizes another geometric principle referred to as arcual displacement amplification, dispayed in Figure 2. Displacement of a lever close to its hinge results in larger displacement further from its hinge. Equation 3 demonstrates this relationship [2].

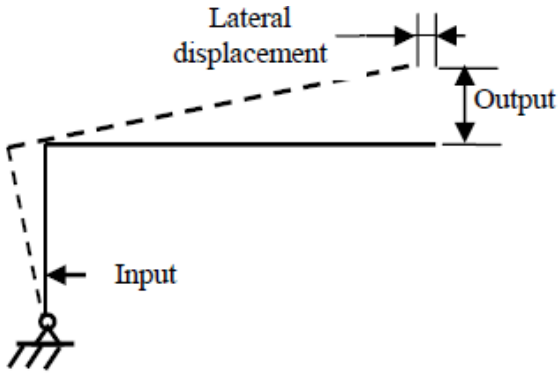

Figure 2: Arcuate Displacement Amplification Principle [3]

$$\delta_{out} = \frac{l_{out}}{l_{in}} \delta_{in} \tag{3}$$

Above, l_{out} is the distance from the hinge in which the output displacement is measured, and l_{in} is the distance from the hinge in which the input displacement is measured. Pythagorean and arcual displacement amplification are the two geometric principles constituting the basis of three fundamental displacement geometries: bridge, lever, and four-bar.

2.1.3. The Fundamental Bridge Geometry

The first elementary mechanical displacement geometry is the bridge amplifier. The bridge utilizes the Pythagorean amplifying principle on two symmetric linkages for amplified displacement in a transverse direction, as demonstrated by Figure 3. MDA configurations often position two bridges in parallel to

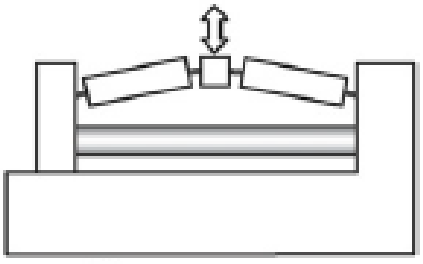

Figure 3: Bridge Displacement Amplifier [4]

double the transverse displacement; Figure 4 exhibits the three common types of double bridge structures.

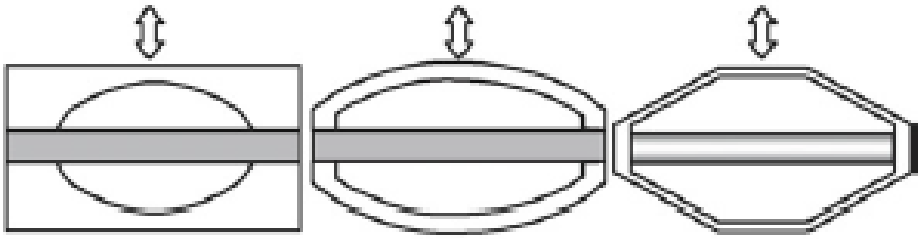

Figure 4: Moonie, Rainbow, and Cymbal Type Bridge Amplifiers (left to right) [4]

These mechanisms induce a vertical displacement in response to a lengthening by the darkened center bar (commonly a piezoelectric material). The Moonie-Type mechanism was developed in 1992 by Niezrecki et al. Increases in the cavity diameter and depth maximize output. Furthermore, a minimization in thickness at the center and endcaps achieves the highest gain [5]. The Rainbow-Type and Cymbal exhibit a large potential displacement output via a combination of flexural and rotational motion. However, the thin beam structures of these mechanisms are susceptible to instability at high frequencies [4]. Figure 5 shows a more detailed view of the Cymbal mechanism.

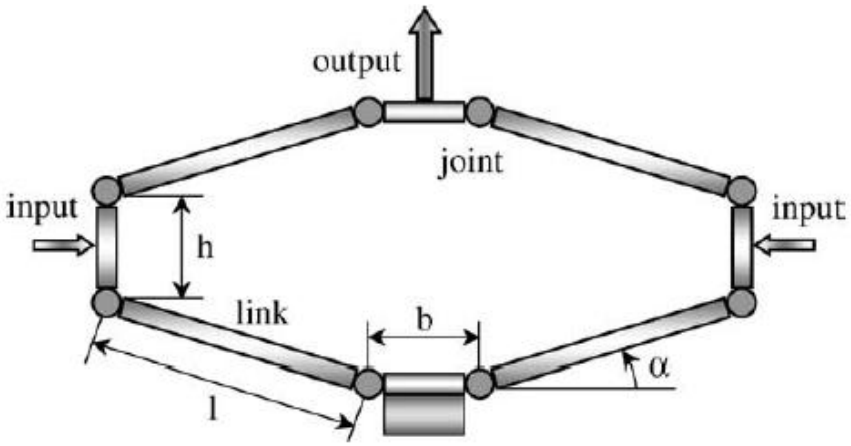

Figure 5: Cymbal-Type Displacement Amplifier [6]

The figure above consists of four biaxially symmetric right triangles connected via rolling joints in a Cymbal-Type mechanism. The input reduction of the long leg of each right triangle directs an amplified output increase in the length of the short legs. Lobontiu et al. [2] analytically determined the amplification ratio of this mechanism as expressed by equation 4:

$$AR = \frac{\sqrt{l^2 (\sin\alpha)^2 + \delta_{in}(2l\cos\alpha - \delta_{in})} - l\sin\alpha}{\delta_{out}} \quad (4)$$

As shown, instantaneous amplification ratio increases with linkage length *l*, but decreases with input displacement δ_{in} and angle α. However, large linkage length may result in unwieldy mechanisms with a large natural frequency. Furthermore, a reduction in the initial angle of the linkages increases the necessary force associated with the input displacement and increases stresses at the joints. Upon construction of bridge mechanisms, these parameters must be optimized considering the force input and displacement of any specific application. The involvement of input displacement δ_{in} in the amplification ratio equation demonstrates that the bridge mechanism is most effective at small displacements. Benefits of this technology include

its simplicity and durability under high stress. In addition, the bridge mechanism benefits from its symmetrical structure, providing high gain, precise, linear output motion [6]. On the negative side, the joints and pseudo-static boundaries of an MDA absorb a large portion of the input force in bridges with small angles. This results in high stress in the linkage and joints, as well as low force transmission. The bridge mechanism in itself is useful for low displacement input amplification where force transmission efficiency is less important. A plethora of MDA arrangements utilize the fundamental bridge geometry, as it is one of the most basic building blocks of displacement amplification.

2.1.4. The Fundamental Lever Geometry

The lever displacement amplifying mechanism utilizes arcuate displacement amplification. Figure 6 depicts this mechanism. The lever running across the top of the mechanism hinges at the left side. The actuator on the left induces displacement close to the hinge, so that the right side of the lever is displaced an amount proportional to its distance from the hinge l_{out} compared to the input displacement's distance from the hinge l_{in}.

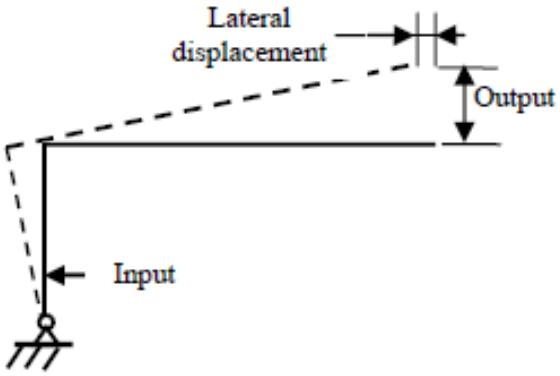

Figure 6: Lever Displacement Amplifier [3]

$$AR = \frac{l_{out}}{l_{in}} \tag{5}$$

The simple lever MDA demonstrates large gain at high force transmission efficiency, since there is only one hinge within the structure [6]. Flexure-based hinges absorb energy; minimization of the number of hinges in an MDA maximizes force transmission efficiency. An undesirable aspect of the lever mechanism is the arcuate rather than linear displacement. For applications that require purely linear output, the lever tacks on lateral displacement that may hinder energy generation. The two-bar lever amplifier in Figure 6 illustrates this lateral displacement.

In conclusion, circumstances that require high amplification ratio and force transmission should utilize the lever mechanism, since the low number of hinges reduces the amount of energy that is stored. However, for precision-oriented mechanical displacement amplification applications, the lateral displacement associated with the output displacement pose an issue.

2.1.5. The Fundamental Four-Bar Geometry

The four-bar displacement amplifier is the third fundamental geometry utilized in many MDA structures. It takes advantage of the geometric principles of two right triangles to induce amplified transverse displacement in response to mechanical input, as shown in Figure 7.

Figure 7: Four-Bar Displacement Amplifier [8]

MDA configurations requiring special output movements largely utilize the four-bar mechanism for its precision-oriented and high-gain displacement amplification capabilities [6]. However, in some configurations the four-bar mechanism will produce lateral displacements. Ouyang [3] ameliorated the issue of lateral displacement within the four-bar mechanism by introducing the double-symmetric parallel four-bar topology. With his design, Ouyang demonstrated the valuable aspects of the four-bar structure if it is modified to eliminate the transverse displacement. Their structure also demonstrated a high stiffness and natural frequency, which is generally desirable for non-resonant MDA's [3]. A disadvantage to a compliant four-bar mechanism is the large number of energy-absorbing flexure hinges, reducing overall force transmission efficiency. High displacement, high precision applications that do not require significant force transmission should utilize the four-bar mechanism.

2.1.6. The Buckling Beam

The above geometric principles and mechanical structures are heavily utilized throughout a large portion of mechanical displacement amplification mechanisms; however, they do not constitute the entire spectrum of structures within this field. Structures such as the buckling beam, hydraulic mechanism, pantograph, and others utilize the above geometric principles in addition to things such as material elasticity and fluid flow in order to amplify displacement in creative ways. The following review will discuss a variety of specific displacement amplification mechanisms in order to analyze their detractions and benefits in the context of small-scale energy generation.

The buckling beam is similar to the bridge structure previously discussed, but it uses the elastic properties of a material to bend in an almost uniform arc, as opposed to the bridge mechanism that bends at specifically designated joints. A slender beam will buckle when subjected to a critical compressive force:

$$P_{cr} = \frac{H\pi^2 k}{L^2} \tag{6}$$

H is a constant dependent on the boundary conditions of the beam, and the constant k is the minimum flexural rigidity of the beam [9]. The large input force required to buckle the beam is the principle disadvantage to this displacement amplification mechanism. For this reason, only situations associated with a high compressive force may utilize the buckling beam. However, the introduction of an initial imperfection, such as a slight curve in the beam, mitigates this issue. Considering a curved imperfection modelled using a sine curve with an amplitude of ζ/2, Saif and Macdonald [9] analytically determined the reduction in critical force to be the following:

$$\frac{P}{P_{cr}} \approx \left(1 - \frac{\zeta}{D}\right) + \frac{\pi^2 D^2}{8L^2}\left(1 - \frac{\zeta}{D}^3\right) + \frac{3}{64}\left(\frac{2\pi}{DL}\right)^4 \quad (7)$$

Thus, subjecting the geometry of the beam to an initial imperfection can significantly decrease the critical buckling force required for deformation. Furthermore, an initial imperfection practically has no effect on the output displacement of the buckling beam [9].

Despite the issues associated with the threshold buckling force, buckling beams exhibit significant output. Amplification Ratio (AR) is the primary parameter used to analyze the effectiveness of a displacement amplifier; it is simply the ratio of output displacement to input displacement. Saif and Macdonald [9] determined the amplification ratio of a fixed-end buckling beam to be the following:

$$AR = \frac{2L}{\pi^2 D} \quad (8)$$

L is the length of the beam and *D* represents its current axial displacement. Clearly, the amplification ratio of a buckling beam is inversely proportional to its current axial displacement. However, the buckling force required significantly drops after initial longitudinal displacement. Considering these correlations, the buckling beam is most effective for applications of high force and small displacement. The beam may not react to a small force, and for large input displacement, the amplification ratio becomes too small. Buckling beams provide high displacement amplification in response to large compressive force at small displacements.

2.1.7. The Hydraulic Mechanism

The hydraulic displacement amplification mechanism (HDAM) takes advantage of differing cross-sectional areas in the displacement of hydraulic fluid in order to obtain a displacement gain. Many HDAM's exist as varieties of the following basic structure: there is a cavity filled with some fluid, defined by a few basic characteristics. The fluid must have a low bulk modulus so that it is incompressible in response to displacement input. The fluid should have low viscosity to avoid energy losses due to molecular shear stresses. Finally, it should have a low freezing point to allow for application in a range of environmental conditions. The cavity will have two pistons. The input piston should have a large cross-sectional area in contact with the fluid cavity, while the output piston has a small cross-sectional area. A water sealing film on the pistons blocks leakages. This structure is exhibited by Hwan-Sik Yoon, et al. [10] in his experiments on using hydraulic amplifiers to enhance piezoelectric strokes.

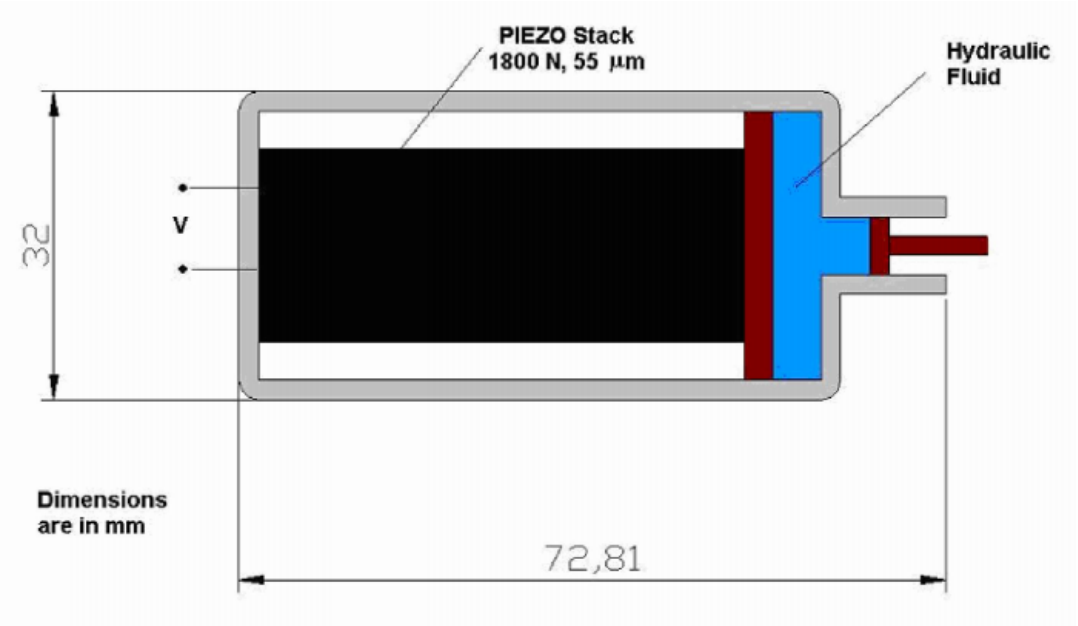

Figure 8: Hydraulic Displacement Amplifier [10]

Depicted in Figure 8 is the most simplistic of hydraulic amplification structures. Assuming the mechanism's cross-section is circular, the output piston's ideal displacement depends on the ratio of the input and output cross-sectional areas:

$$AR = \frac{{D_{in}}^2}{{D_{out}}^2} \tag{9}$$

D_{in} and D_{out} are the diameters of the input and output pistons, respectively. While an ideal hydraulic amplifier adheres to the above relationship, HDAMs are often inefficient due to a variety of fluidic properties. For example, Yoon et al.'s experiment on the above HDAM measured only 40% of the designed stroke and a very low force transmission.

Losses within this mechanism are a result of a variety of factors. The compliance of internal parts can induce friction and/or plastic deformation. One must fabricate HDAMs with very low geometric tolerances, tight water seals, and lubrication in order to alleviate some of the effects associated with this. Furthermore, no fluid has an infinite bulk modulus. Compressibility in a hydraulic fluid reduces gain. Finally, viscous effects within the fluid cavity absorb energy and result in unpredictable mechanism responses. All of these factors contribute to the reduction of gain in hydraulic displacement mechanism amplifiers. However, Ninomiya et al. [11] found a way to minimize many of these factors in the construction of a microelectromechanical system utilizing the principles of hydraulic displacement.

In an experiment conducted by Ninomiya et al., a MEMS-based HDAM was constructed for the purpose of amplifying piezoelectric displacement for tactile displays. This design addressed many of the shortfalls associated with Yoon et al.'s [20] HDAM. This mechanism consisted of a glycerin-filled microcavity completely sealed within an easily deformable, elastic membrane encapsulated in silicon wafers, as depicted in Figure 9.

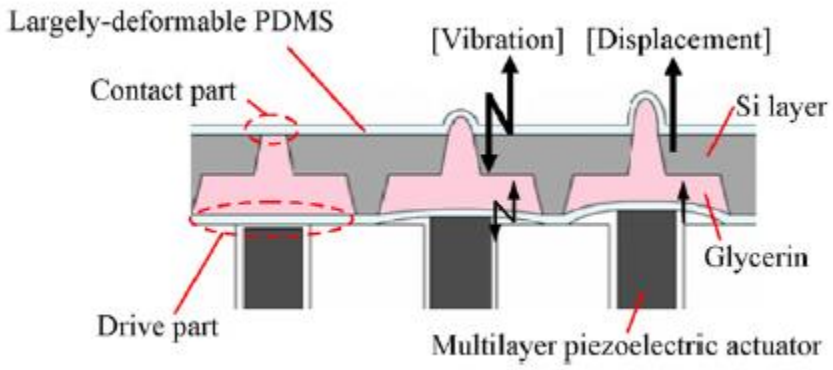

Figure 9: MEMS Based Hydraulic Displacement Amplifier [11]

This design exhibited an amplification ratio of 15 in response to input displacement by a piezoelectric actuator. Figure 10 demonstrates an interesting correlation yielded by this study: as the size of the contact parts decreased, amplification ratio increased. This indicates that further miniaturization of the hydraulic amplification mechanism would result in greater amplification ratios. This is probably because a minimization of the volume of a fluid simultaneously decreases the impact of fluid compressibility. Furthermore, flow remains laminar in miniaturized cavities, reducing shear stresses associated with turbulence,

Another peculiar result of this study was the effect of opening diameter on amplification ratio. One would think that a larger opening diameter would result in a larger amplification ratio, since AR is a result of the ratio of cross-sectional areas. However, this experiment found an optimal opening diameter in 660 μm, as exhibited by Figure 11, after which AR begins to decrease. This result further enforces the principle that small-scale systems should use hydraulic amplifying mechanisms. Initially, as opening diameter increases the AR increases due to the increase in the ratio of cross-sectional areas. However, as the opening diameter becomes too

large the loss-inducing factors of compressibility and fluid viscosity dominate and reduce the gain [10].

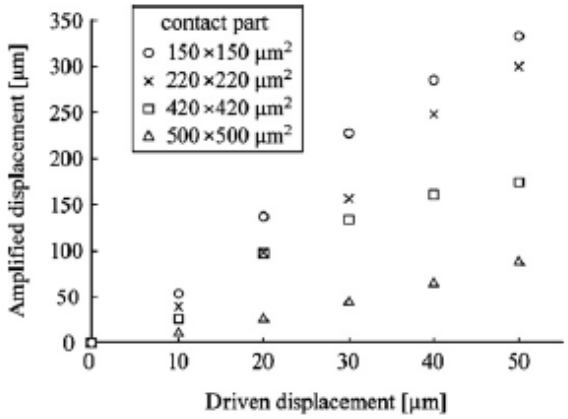

Figure 10: Contact Part Size and AR [11]

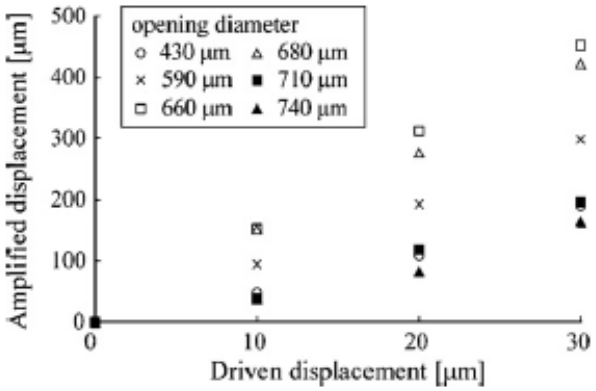

Figure 11: Opening Diameter and AR [11]

The above analysis yields the following conditions necessary for the construction of a high-gain hydraulic displacement amplifier. First, the hydraulic fluid should possess a high bulk modulus, low viscosity, and low melting point. Ninomiya et al. [11] demonstrated the value of glycerin as a working fluid in these mechanisms. A maximization of output piston area to input

piston area will generally optimize gain. One must completely seal fluid cavities to avoid leakage. However, the introduction of a membrane reduces force transmission through its elastic resistance to deformation. Finally, these systems are most valuable on the very small scale in order to negate the effects of compressibility and viscosity in the working fluid.

If force transmission is an essential parameter in a design, one should use hydraulic mechanisms primarily for small-scale displacement amplification. However, if a loss of force gain is tolerable in an application, large and bulky hydraulic mechanisms can obtain a very large amplification ratio. In these applications, such a mechanical amplifier is slow and bulky. Hydraulic displacement amplification mechanisms prove to be useful for a variety of applications; however, the incorporation of fluid dynamics in a mechanical system introduces a slew of potential sources of loss.

2.2. Flexure Hinges

In designing mechanical displacement amplifiers, in addition to the design of a specific geometry of linkages to produce output displacement gain, one must consider the connectivity between these linkages in order to ensure smooth rotation with a minimization of energy loss. There is a variety of connective possibilities: rotation joints, rolling joints, flexure hinges, etc. This section will focus on the flexure hinge, as it has a plethora of benefits for micromechanical mechanisms.

First, flexure hinges enhance manufacturability in a micromechanical mechanism. Without joints, pins, or notches, an MDA can be 3-D printed from a single stock of material.

This vastly simplifies the fabrication process and reduces required maintenance. Furthermore, the 3-D printing of a compliant mechanism allows for compactness and complexity in the design. A mechanism without separate parts has fewer stress concentration factors, which leads to increased strength and durability. As opposed to rotational joints, flexure hinges experience no friction losses or need for lubrication. There is no hysteresis associated with the flexure hinge. A detriment associated with hinges is the energy absorption associated with their plastic deformation. Hinge stiffness is inversely proportional to amplification ratio in compliant MDA's. For many applications, compliant mechanisms utilizing flexure hinges are generally superior to mechanisms with multiple machine parts connected via pins and rolling joints. Within the field of flexure hinges there are many possibilities. The main ones to consider are the right circular hinge and the corner-filleted hinge [6].

2.2.1. The Right Circular Hinge

The right circular hinge is the simplest flexure hinge. All bending occurs at the middle of the hinge and thus the essential parameters are hinge thickness and length, as outlined in Figure 12. In an examination of a flexure hinge's impact on amplification ratio, it's torsional spring constant is the essential parameter. This value depends on modulus of elasticity, thickness, width, and radius as detailed in the equation first published by Paros and Weisbord [12]:

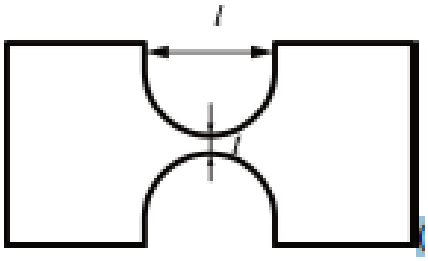

Figure 12: Right Circular Flexure Hinge [2]

$$K = \frac{2Ebt^{5/2}}{9\pi R^{\frac{1}{2}}} \quad (10)$$

This equation demonstrates the importance of flexure hinge thickness on the materials resistance to rotation. The spring constant should be generally be minimized; however, as spring constant is reduced so too does natural frequency decrease. In many applications it is beneficial for a mechanism to possess a high natural frequency. In 1996 Xu and King [7] analyzed circular, corner-filleted, and elliptical flexure hinges to determine that circular hinges had the highest stiffness, though they produced the most reliable and controlled motion. The right circular hinge should be used for high-frequency applications that require small displacement with high precision.

2.2.2. The Corner-Filleted Hinge

The corner-filleted hinge is somewhat of an opposite to the right circular hinge. It is long and thin, and filleted where it meets with the linkage. It demonstrates a much lower stiffness and thus exists in mechanisms of a lower natural frequency.

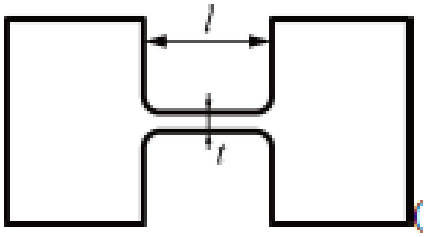

Figure 13: Corner-Filleted Flexure Hinge [4]

Paros and Weisbord [12] in 1965 found that the torsional spring constant of this type of hinge also depended most heavily on hinge thickness:

$$K = \frac{Ebt^3}{12(l - 2r + 2rf(s))} \quad (11)$$

$$s = \frac{2r}{t}, f(s) = \frac{(2s+1)(3s^2+2s+1) + 3s(s+1)^2\sqrt{2s+1}\tan^{-1}\sqrt{2s+1}}{(s+1)(2s+1)^3}$$

With lower stiffness, corner-filleted flexure hinges demonstrate less precision in terms of rotation. This means that often corner-filleted hinges deviate from the rotation center point. This issue could be negated considering geometrical supports within the device, but axial torque would impart greater stresses on the hinge and increase the fatigue over time. The corner-filleted hinge should be used for higher rotational displacement, where accuracy and stability is less important. The highest relative accuracy of corner-filleted hinges occurs when the fillet radius is 5% of the hinge length [8].

2.2.3. Double Flexure Hinge

Double flexure hinges offer unique benefits in terms of stiffness and durability. In experiments conducted by Ouyang et al [3]., the double flexure hinge demonstrated a lower stiffness than a single corner-filleted hinge with a thickness equal to the sum of the thickness of the double hinges. Mathematically this is logical, considering the equations developed by Paros and Weibord in which $K \alpha t^{5/2}$. In turn, double corner-filleted flexure hinges exhibited higher precision than single flexure hinges. Since flexure hinge stiffness is inversely proportional to amplification ratio, mechanical amplification devices utilizing the double flexure hinge structure exhibited greater amplification ratios [12].

Figure 14: Double Corner-Filleted flexure Hinge [3]

2.2.4. Natural Frequency

The natural frequency of a displacement amplification device must be optimized if it is to be used for energy generation; thus, the flexure hinge stiffness must be carefully considered. Flexure hinge stiffness is most dependent on the thickness of the hinge, so an analysis of hinge thickness compared to natural frequnecy is the most telling indicator of how to optimize natural frequency. Ouyang et al. [3] conducted a study on how the thickness of a hinge impacts natural frequency of double-symmetric four bar mechanical amplification mechanism utilizing corner-filleted hinges. The results in Table 1 demonstrate how hinge thickness impacts amplification ratio and natural frequency [3].

Table 1: Hinge Thickness, AR and Natural Frequency [11]

Thickness of the flexural hinge (mm)	Amplification ratio	Natural frequency (Hz)
0.3	24.9	458.5
0.4	21.6	491.9
0.5	18.5	532.9

2.2.5. Flexure Hinge Material Considerations

In addition to thickness, the materials used for flexure hinges largely impact important output parameters; one should minimize the Young's Modulus of a flexure hinge material to enhance amplification ratio, but not so much that the mechanism becomes destabilized. Hinge material consideration is a precarious balance. Flexure hinges will probably be comprised of steel, titanium, or aluminum with Young's modulus values of around 210, 110, and 70 GPa,

respectively. As previously stated, materials with a higher stiffness are more efficient in transmitting force. Furukawa et al. [13] quantified these values in an analysis on flexure hinges for piezodriven mechanisms. That study found the force transmission efficiency limits of such materials to be 81%, 71%, and 49%, respectively, for a simple lever amplifier [13]. A high Young's modulus flexure hinge results in higher tensile stress, which can cause problems in durability and plastic deformation. Too low a Young's modulus can diminish the output force and displacement of the mechanism but reducing the overall stiffness. According to Furukawa [13], for many applications titanium represents the balanced and optimal choice. Furthermore, titanium is desirable for this specific application. It has low magnetic properties, so it will be less affected by electromagnetic energy generating mechanisms. It also has a very high density and strength. Finally, the endurance limit of the material is essential. If the MDA is to be durable over many cycles, the endurance limit of the material should exceed the maximum stress. Nikolas Hrabe et al. [14] measured an endurance strength of over 550 MPa in titanium alloy Ti-6Al-4V after the hot isostatic pressing process.

2.3. Ambient Energy Generation

The increasing ubiquity of powered mechanisms from sensors on bridges to rotation control in prosthetic limbs necessitates the availability of decentralized energy sources. The methods of ambient kinetic energy harvesting generally require efficient mechanical displacement amplification, so these two topics fit neatly together. This section will discuss a

variety of methodologies for producing wattage on a small scale from otherwise dissipated kinetic energy.

2.3.1. Piezoelectric Transducers

Piezoelectric ceramics are a unique subset of materials that can convert mechanical stress to functional voltage. The piezoelectric effect is a polarizing response that non-centrosymmetric materials exhibit in response to applied mechanical stress. The voltage developed by said polarization can be utilized to charge a capacitor or battery. Surface charge polarization is generalized as a linear process represented by the following formula:

$$D = \varepsilon E \tag{12}$$

where D is the displacement of charge density [$\mu C/cm^2$], ε is the permittivity of the piezoelectric material, and E is the electric field [15]. This equation is an ideal representation of charge displacement; in reality, the developed voltage depends on many extraneous factors such as crystal defects and free carrier density in the material. Orientation of the polarization field can be determined through examination of the material's crystal symmetry; this depends on the alignment and strength of applied mechanical deformation. The fundamental linear piezoelectric equation is expressed in equation 13:

$$D = d * T + \varepsilon^T * E \tag{13}$$

where the variables from above hold the same, d is the piezoelectric charge constant, T is applied mechanical stress, S is mechanical strain, E is the electric field vector, and ε is permittivity at constant mechanical stress [1]. The derivative of the above equation with respect to time

indicates that the rate of stress application affects the rate of displacement of charge displacement as outlined by equation 14:

$$I = d * \left(\frac{dT}{dt}\right) \tag{14}$$

in which I is the induced current in the material and is the same as *dD/dt.* T is again the rate of applied stress [15]. In summation, total voltage in the piezoelectric material depends on the magnitude of stress application, the induced current depends on the rate of stress application. These relationships indicate that piezoelectric materials are valuable for low-displacement, impulse-based energy harvesting.

As exhibited above, piezoelectric materials output high voltage in response to mechanical stress; however, issues associated with piezoelectric energy harvesting are numerous. First and foremost, the maximum strain for piezoelectric materials is low. They are ceramic materials and exhibit their characteristic brittleness. Therefore, for applications experiencing high force input, regular maintenance is required to replace fractured crystals. Furthermore, the development of free carriers and subsequent screening in piezo-materials poses an impediment to the development of larger voltages. These charge carriers rapidly move throughout the material in response to the resultant electric field and screen the produced voltage. This screening occurs within nanoseconds of the generation of the electric field, and thus is detectable only through an experimental voltage reduced from theoretical values [15]. The presence of screening in piezoelectric materials can be partially suppressed with a rectifying (Schottky) barrier at one electrode contact. Furthermore, screening can be prevented through careful synthesis of piezo-electric materials. Various fabrication methods can serve to minimize carrier density in synthesized materials. These methods include oxygen plasma treatment to reduce surface

defects, the introduction of acceptor-type dopants to compensate for intrinsic defects, and surface passivation using oleic acid [15].

Despite these limiting issues, Xu et al. [16] constructed a PMN-PT nano-wire based polymer nanocomposite that showed a measured output of 7.8 V, one of the highest voltage outputs measured using piezoelectric harvesting techniques. These researchers addressed the brittle nature of these materials by embedding the piezo-nanocrystals in a polymer-based nanocomposite designed to absorb superfluous displacement. The researchers managed to minimize displacement absorption by the polymer just enough to produce viable voltage output. Figure 15 illustrates the results of this experiment which induced the polymer to mechanical tapping at half-second intervals.

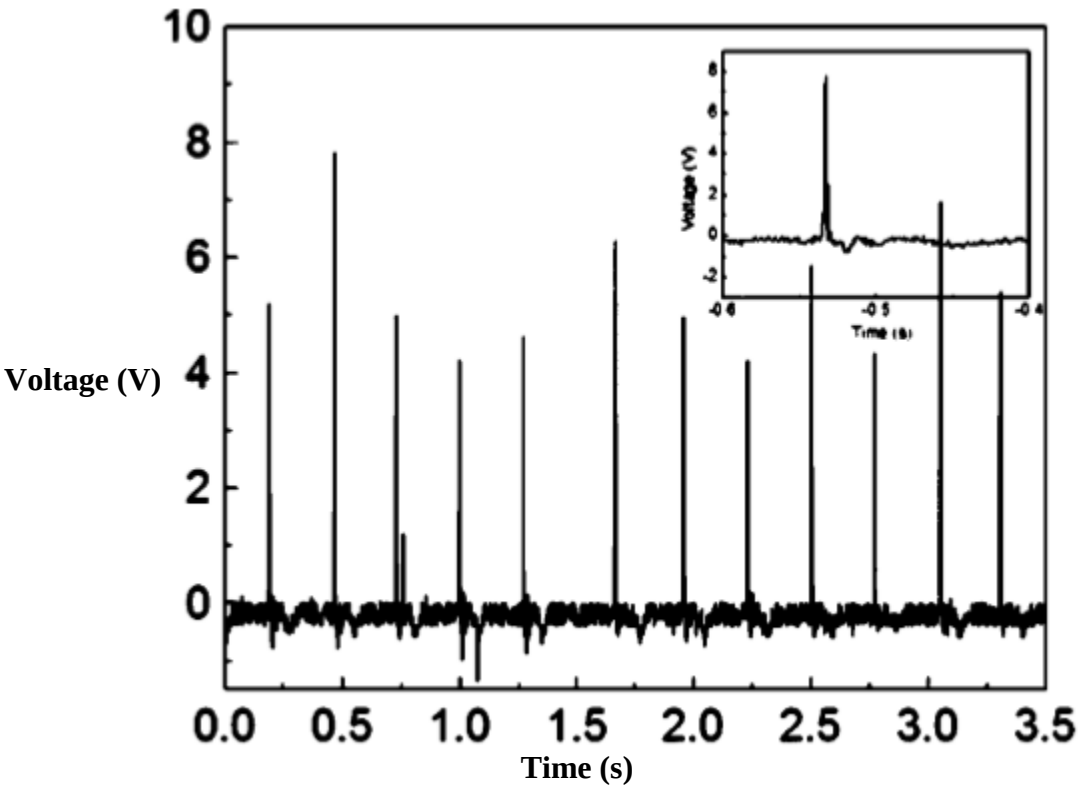

Figure 15: Voltage Response of PMN-PT Nano-wire based Piezoelectric to Mechanical Tapping [16]

2.3.2. Electromagnetic Induction

A changing magnetic field in a closed, conducting loop induces a current; this is the simple concept behind energy harvesting via Faraday's Law of magnetic induction. An electromagnetic transducer aims to convert vibrational displacement to electrical energy by directing mechanical input to a magnet within a coil. When the magnet is displaced, magnetic field within the coil changes, and induces a current in the coil. A battery or capacitor integrated into the circuit produces a usable voltage.

Various studies have demonstrated somewhat effective means for harvesting energy via the linear displacement of a permanent magnet within a coil. For example, Duffy and Carrol [17] generated a root mean square 500 mV in an open circuit through the integration of an electromagnetic generator in a shoe sole. In 2011, Bouendeu et al. [18] constructed a small high performance electromagnetic generator that supplied a 500 Ω load with 422 μW of electrical power. This may seem like a small power output, however the generator weighed only 12.7 g and was 24 mm in length. Generators on a larger scale would have a greater output.

In the above study, Bouendeu derived some useful equations for the open circuit voltage and the electrical power output of a linearly oscillating electromagnetic generator:

$$V = \frac{k_{em}\omega^3 Y_0}{\sqrt{(\omega_0^2 - \omega^2)^2 + (2\xi_m\omega_0\omega)^2}} \tag{15}$$

$$P_{out} = \frac{R_L(k_{em}\omega^3|Y_0|)^2}{2((R_L + R_i)^2(L\omega)^2)((\omega_0^2 - \omega^2)^2 + (2(\xi_e + \xi_m)\omega_0\omega)^2)} \tag{16}$$

where k_{em} and ω_0 are, respectively, the electromagnetic coupling factor and resonant frequency of the generator. ξ_e and ξ_m represent the electrically induced mechanical damping ratio and pure

mechanical damping ratio of the generator. Y_0 is the amplitude of the oscillation, L is the inductance of the coil, and R_L and R_i are respectively the resistance of the load and the coil.

These equations provide an indication of the essential parameters to analyze in constructing a linearly oscillating electromagnetic generator. For example, a greater frequency and amplitude will provide a greater power output, obviously. Furthermore, mechanical damping should be minimized through the reduction of friction and other sources of loss in a generative mechanism. These equations also indicate the importance of maintaining an operating frequency as close to resonance as possible. This poses an issue. For deriving power based on an irregular mechanical input, such as human motion, a device must be constructed that can vibrate with a large amplitude at a diverse bandwidth of frequencies.

In 2008 Saha et al. [19] ventured to tackle this very problem, constructing a linearly oscillating electromagnetic generator that produced power at a variety of bandwidths. The design placed an oscillating permanent magnet within a tube bounded by stationary permanent magnets to act as magnetic springs, as pictured in Figure 16.

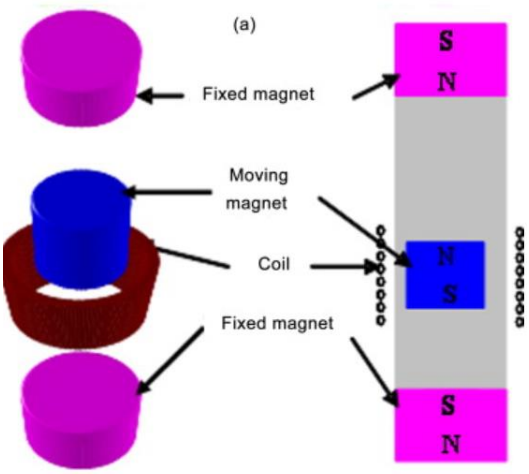

Figure 16: Magnetically Bound Linear Electromagnetic Generator [19]

Saha et al [19] determined a few methods of maximizing power generation within the design illustrated in Figure 15. First of all, flux linkage can be increased through using not just one oscillating magnet, but two magnets glued together and separated by a soft pole piece. Field plots of the peak flux density of the double magnets showed that this configuration exhibited a flux density almost twice as much as the single magnet. Furthermore, the magnitude

of the oscillation was enhanced through the removal the top magnetic spring. This reduced the natural frequency of the magnet oscillation and increased the amplitude. [19].

The power output of the revised generator is exhibited in Figure 17. Peak no-load voltage at resonance frequency is shown to be around 2 V, although at frequencies farther from resonance the voltage is still about 1 V. The prototype also generated 0.3-2.46 mW of power when placed in a backpack during walking and slow running. These values demonstrate the feasibility of power generation by linear oscillation of a magnet within a coil.

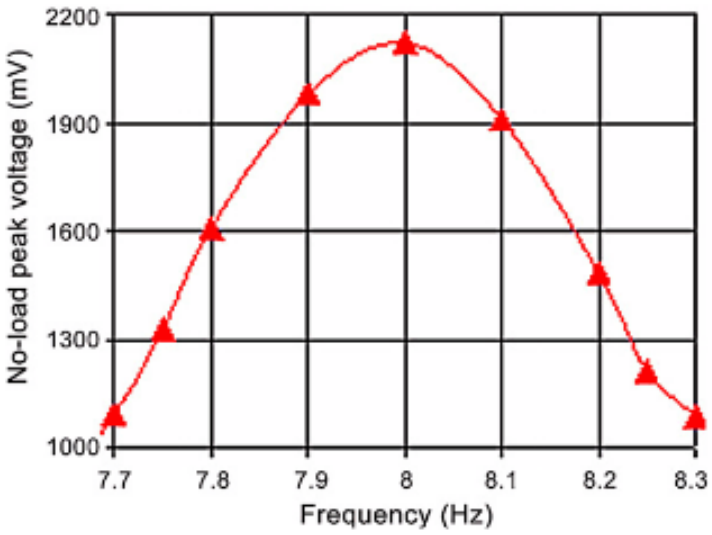

Figure 17: No-Load Peak Voltage for Revised Electromagnetic Generator [19]

The advantages of electromagnetic devices for harvesting energy are numerous. They demonstrate high output currents and are a proven, utilized technology. They are robust and durable. These generators can utilize both rotational and linear mechanical input. However, many of the above studies demonstrate low output voltages and even lower power supply. These low outputs are largely due to the small size of the generators; it is difficult to develop powerful MEMS devices utilizing electromagnetic induction. Output for these devices is poor at low frequencies, and it is difficult to develop a device that operates under a range of bandwidths. The above studies have demonstrated some valuable characteristics to include in the development of such a generator. In deriving energy from an irregular mechanical input, oscillation amplitude is essential. One must reduce mechanical damping in as many forms as possible so that magnetic

damping is the only resistive force in the mechanism. Instead of one magnet, two magnets separated by a 3 mm pole piece will produce a larger flux linkage. Finally, the size of the generator is of utmost importance. To derive reasonable output power, a generator should at least be on the decimeter scale.

Chapter 3

Preliminary Design

3.1. Theoretical Design

The design of the mechanical displacement amplifier relies on two fundamental amplification mechanisms previously discussed in the literature review: the lever mechanism, and bridge or buckling beam. In addition, it heavily relies on the flexure-based properties of titanium; however, the more complicated material properties will be omitted from a theoretical discussion of the design. A simplified model of the design principles behind the mechanical displacement amplification mechanism is depicted in Figure 18.

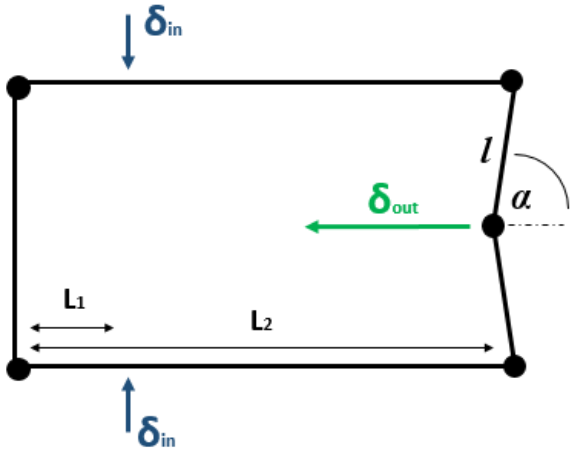

Figure 18: Simplified MDA Design

As illustrated above, the displacement input is directed at the hinge of a lever amplifying mechanism. At the right-hand side of the lever, the displacement δ_{lever} is exhibited by equation 18:

$$\delta_{lever} = \frac{L_2}{L_1}\delta_{in} \tag{18}$$

This displacement is transferred to the bridge mechanism on the right-hand side, which uses Pythagorean amplification principles to produce displacement gain according to equation 19:

$$\delta_{out} = \sqrt{l^2\,(\sin\alpha)^2 + \delta_{lever}(2l\cos\alpha - \delta_{lever})} - l\sin\alpha \tag{19}$$

So, the total displacement as a function of input displacement can be represented as the following:

$$\delta_{out} = \sqrt{l^2\,(\sin\alpha)^2 + \frac{L_2\delta_{in}}{L_1}(2l\cos\alpha - \frac{\delta_{in}L_2}{L_1})} - l\sin\alpha \tag{20}$$

As exhibited by the equation above, this amplification design is most effective at large dimension values l and L_2 and a small initial angle α.

The above theoretical analysis demonstrates the parameters that must be maximized or minimized in order to achieve a large amplification ratio (AR). It is by no means a complete analysis of the displacement amplification design, which depends on non-ideal structures such as flexure hinges and general material flexibility.

3.2. Model Design

While the above theoretical design adequately demonstrates the amplification processes utilized in the MDA, it falls short of fully expressing the design principles. A mechanism

composed of linked joints would not possess many of the essential characteristics for the application discussed in the previous section. For example, the actual design must possess elasticity and minimal mechanical damping or internal friction. To achieve this, the lever is not simply a rotating linkage but a curved titanium sheet that flexes on an angle. The device is not a rectangular prism but an elliptical prism to flex elastically and more compactly harbor energy generation technology. It contains an outer shell which serves two purposes: to flex in response to mechanical stress, and to protect the internally located linear actuator. An image of the mechanical amplification design is pictured in Figure 19.

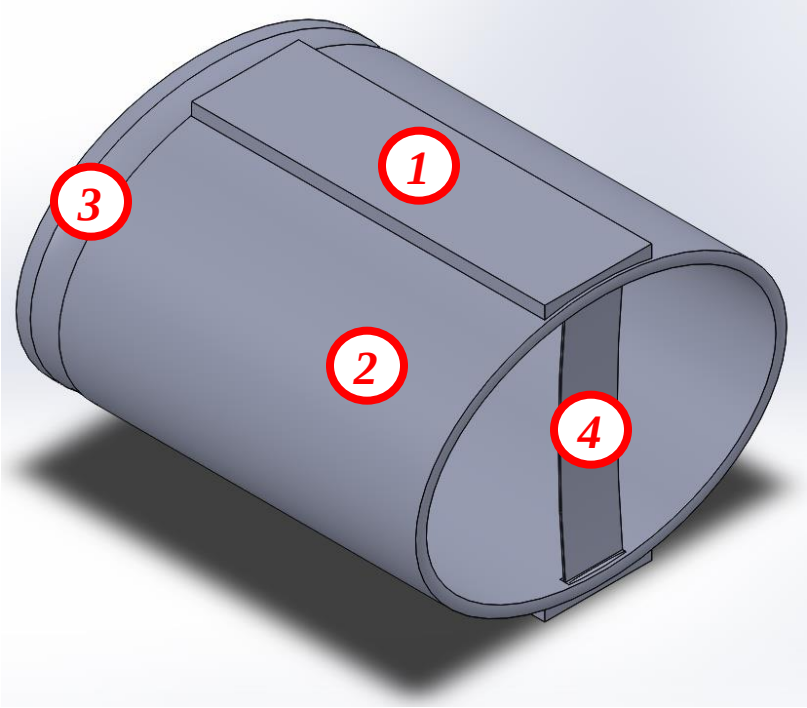

Figure 19: Isometric View of Basic MDA Model

The basic functioning of the MDA is as follows. Force is input to the raised, flat area of Section 1. The thin titanium shell (2) flexes in response to the stress, rotating on flexures hinges at Section 3. The shell acts as a lever amplifying mechanism and transmits force and displacement

to the buckling beam at Section 4. The beam bends in response to the compression. Output displacement is measured at the center of the beam, and input displacement is measured as an average across the surface of the input area 1.

Chapter 4

Methods

4.1. Introduction

Although the theoretical design demonstrates the amplification principles and important variables for the MDA design, proper design of the individual components necessitated a thorough Finite Element Analysis of each component. For example, the distribution of the input force to the displacement amplifier was analyzed to determine how to maximize amplification ratio (AR) and force transmission (FT) via the two flexing levers. Furthermore, the device shape, the bridge/buckling mechanism, and all the flexure hinges were dimensionally optimized through iterative modelling to maximize displacement gain and maintain stability and durability in the structure of the device. Mainly, this analysis process was conducted using Finite Element Analysis in conjunction with Taguchi Analyses to process the variety of variables associated with each aspect of the design. Displacement, force transmission, and maximum Von Mises stress were the essential output parameters considered in each Taguchi Analysis. This section discusses the parameter optimization process associated with each important aspect of the displacement amplifier.

4.2. Input Force Analysis

The proposed MDA was designed to endure about 180 pounds of input force. While the magnitude of this force is constant, the spatial distribution of the force as it encounters the device can be optimized in order to maximize both amplification ratio and force transmission. The following finite element analysis subjected a tentative MDA design to 180 Newtons at a variety of distributions. Of course, for the lever to be most effective, the force must encounter the MDA near the rear where the lever is hinged. So, the input parameter of this analysis was the percentage of the length of the MDA subjected to the input force, beginning from the rear. Figure 20 demonstrates the input and output parameters examined in this portion of the design analysis.

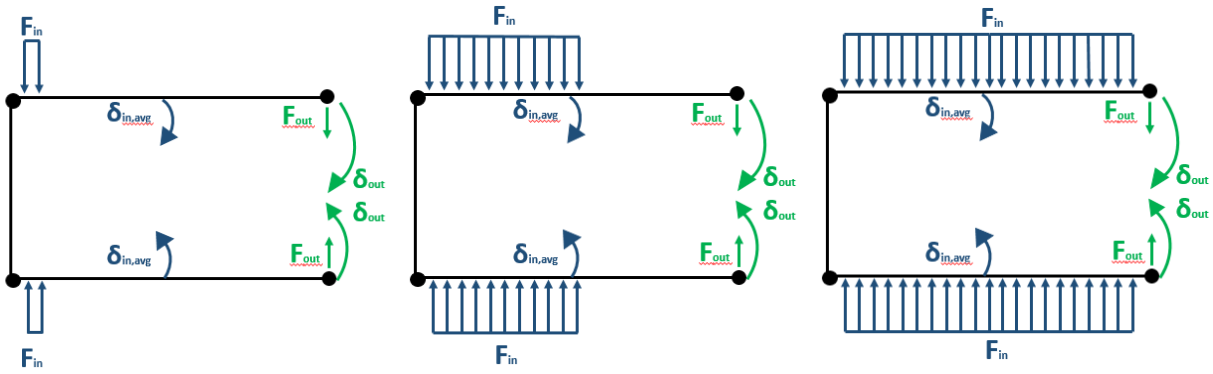

Figure 20: Force Input of 10%, 50%, and 100%, Respectively

Appendix A exhibits the full data table from the finite element analysis associated with input force; however, the plotted results of the study are shown in Figure 21.

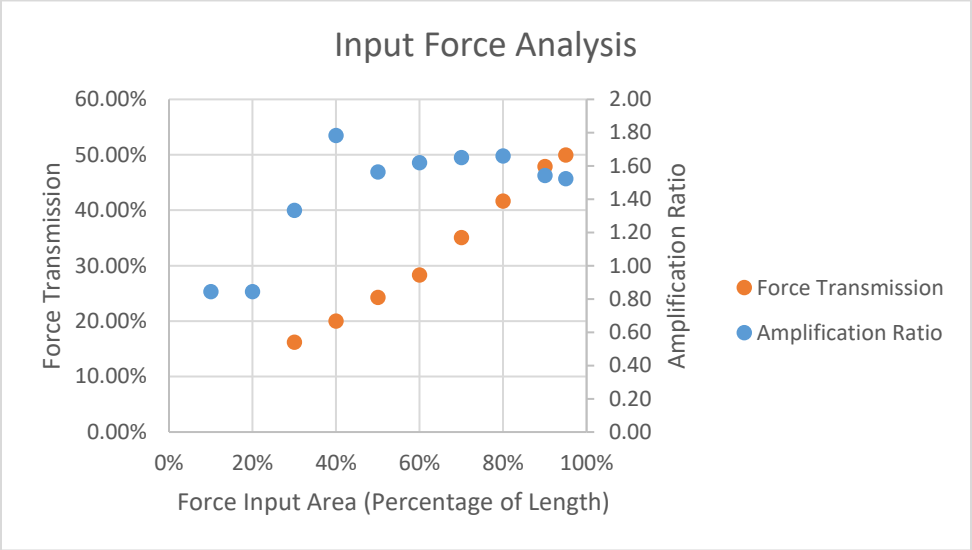

Figure 21: Input Force Analysis

As one can see, the force transmission percentage increases linearly as a function of percentage area. This makes sense, as high percentage force areas transmit force closer to the edge of the lever where the force transmission analysis is taking place. More interestingly, amplification ratio is shown to peak at around 80% input area. This makes sense when looking at the deformation of the finite element models. At very low input area percentages, the lever portion of the displacement amplifier flexes in the middle. This flexure absorbs force energy, thus that energy is not transmitted to the end of the lever where the displacement is recorded. At large input area percentages, the center of force is farther from the hinge of the lever. Keeping in mind the geometric principles governing displacement amplification via levers, a force center farther from the hinge should diminish AR. It appears that 80% force input area is optimal for amplification ratio.

However, one must consider both amplification ratio and force transmission in a design decision regarding force input area. To reconcile the two output parameters, a new variable was

created: amplification ratio/force dissipation, a ratio of the amplification ratio over the amount of force not transferred to the end of the lever. This variable is displayed in Figure 22.

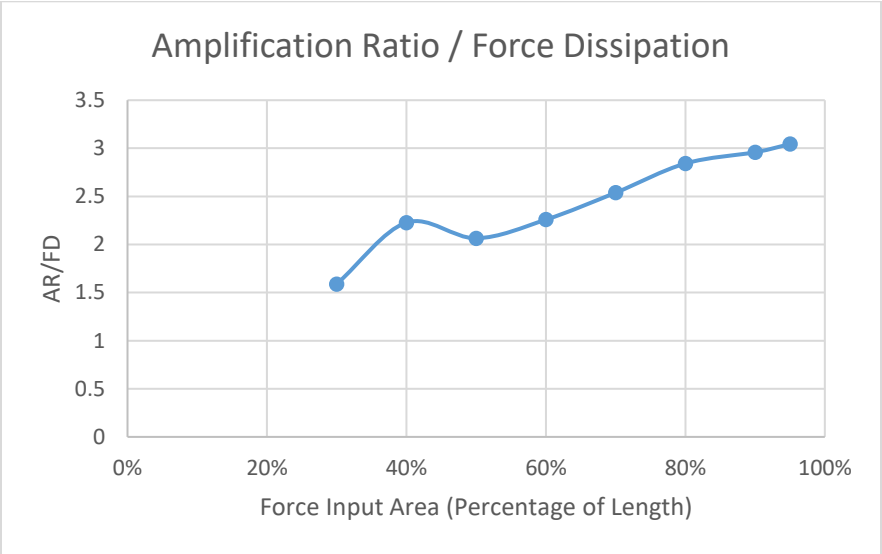

Figure 22: Input Force Analysis, Amplification Ratio / Force Dissipation

The above graph demonstrates that while amplification ratio diminishes at a certain point of force input area, the increase in force transmission overcomes this loss if both parameters are weighted equally. Since 95% force input area demonstrated the largest AR/FD value, the MDA should endure a force across the entire cross-section of its exterior.

4.3. Frame Shape Analysis

The next dimensional aspect of the MDA design to consider is the shape and thickness of the frame. An elliptic prism was chosen for its flexure properties elasticity, and conductivity to integration with energy generation systems. However, there is very little literature available on

how elliptic prisms flex under mechanical stress. So, this portion of the design methodology sought to examine how the ellipsoid's horizontal and vertical radii impacted force transmission and amplification ratio. Figure 23 is a view from the front of the mechanical displacement amplifier; it demonstrates how the frame shape is changing in this portion of the study.

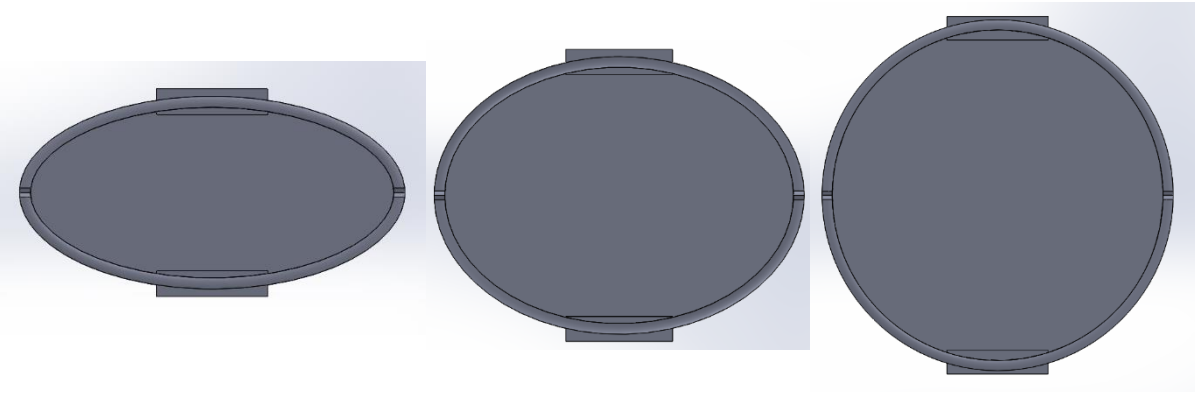

Figure 23: Frame Shapes of 50%, 75%, and 100%, Respectively

The horizontal radius of the ellipsoid was kept constant at 26 mm. The percentage refers to the ratio of the vertical radius to the horizontal radius. Amplification ratio was determined by comparing the average displacement across the top of the lever to the displacement at its free end. Force transmission was determined at the free end of the lever.

In addition to the dimensions of the ellipse, the frame shape analysis considered the thickness of the shell/flexing lever. Since the two shape parameters affect each other, an examination of each could not be conducted independently; an orthogonal Taguchi Analysis was constructed to examine the effect of both aspects of the frame shape on amplification ratio and force transmission. Von Mises stress in the frame need not be considered, as every test demonstrated a stress below the endurance limit of hot isostatically pressed Titanium alloy Ti-

6Al-4V. The full Taguchi Array is included in Appendix B, however its summary is included below in Table 2.

Table 2: Frame Shape Taguchi Analysis

Height-Width Ratio	AR Average	FT Average	Theoretical AR	Theoretical AR/FD
50%	1.78	47.12%	10.10	19.10
55%	1.75	47.18%	10.07	19.07
60%	1.74	47.22%	10.07	19.10
65%	1.72	47.23%	10.05	19.05
70%	1.70	47.37%	10.06	19.11
75%	1.69	47.46%	10.03	19.10
80%	1.67	47.41%	10.00	19.01
85%	1.66	47.23%	9.96	18.87
90%	1.65	47.07%	9.94	18.79
95%	1.64	46.79%	9.91	18.62
100%	1.63	46.69%	9.86	18.49
Coefficient Variation	0.027	0.005	0.007	0.011
Thickness				
1.5	1.76	47.62%	N/A	N/A
3	1.69	47.90%	N/A	N/A
4.5	1.63	45.96%	N/A	N/A
Coefficient Variation	0.031	0.018	N/A	N/A

The Taguchi Analysis tests multiple variables in combination with each other. By averaging the output parameters for each individual input parameter across multiple tests, it provides a good indication of how each parameter independently affects any one output. In addition, the coefficient of variation for each set of output averages exhibits how strongly any one input affects an output.

As shown, as the shape of the ellipse becomes more circular, the amplification ratio decreases. It seems simple, however there is a variable that is not considered in this FEA. The rightward two columns account for this variable. There is a bridge amplifying mechanism after

the lever. As explained in the introduction, the total height of the mechanism is an impactful parameter in the amplification ratio of the bridge amplifying mechanism. So, the "Theoretical AR" column uses equation 19 to predict a theoretical amplification ratio considering the modelled output from the lever as well as the height of the mechanism dictated by the height-width ratio input. When the theoretical amplification ratio is divided by force dissipation, it appears that a height-width ratio of 70% is the optimal shape.

Since the thickness of the frame has no impact on the bridge mechanism, the theoretical amplification ratio is not applicable for thickness studies. In the thickness analysis, both amplification ratio and force transmission concur in an inverse correlation with thickness, so the clear design choice is a minimization of thickness at 1.5 mm.

4.4. Lever Flexure Hinge Analysis

The design is to be compliant, per the benefits of compliant MDA's discussed in the introduction. So, each rotating aspect of the MDA requires a flexure hinge, and there are many options associated with flexure hinges. This section discusses the comprehensive analysis of the type and dimensions of the flexure at the hinge of the lever displacement amplifier.

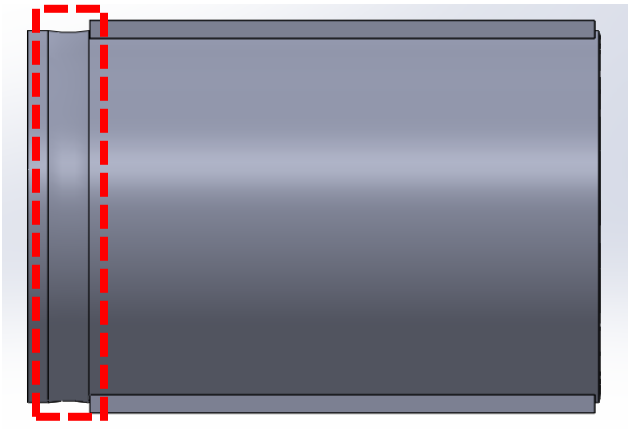

Figure 24: Lever Flexure Hinge

The literature review section already discussed many of the benefits and detractions of various flexure hinge types, so only the few flexure hinges that meet the necessary qualities of the lever hinge were analyzed and modelled. For example, the force transmission of the hinge is essential since the bridge amplifying mechanism depends on a critical input force. Only high force transmission hinges were analyzed. This means that the corner-filleted hinge or double hinge were not considered, while the elliptic and right circular hinges were modelled.

4.4.1. Right Circular Hinge

Right circular hinges have only one parameter to be considered: radius. Since the shell thickness and the flexure width of the hinge are constant in the design, the radius of a right circular hinge determines all other properties. An array of right circular flexure hinges with different radii at the lever hinge was constructed and modelled via finite element analysis, and the resulting amplification ratio, force transmission, and Von Mises Stress at the center axis of the hinge were recorded. Appendix C exhibits the full data results from this portion of the study, and Figure 25 below illustrates graphically the effect of hinge radii on the essential parameters. As every test demonstrated a Von Mises Stress below the endurance limit, stress was not considered in this study.

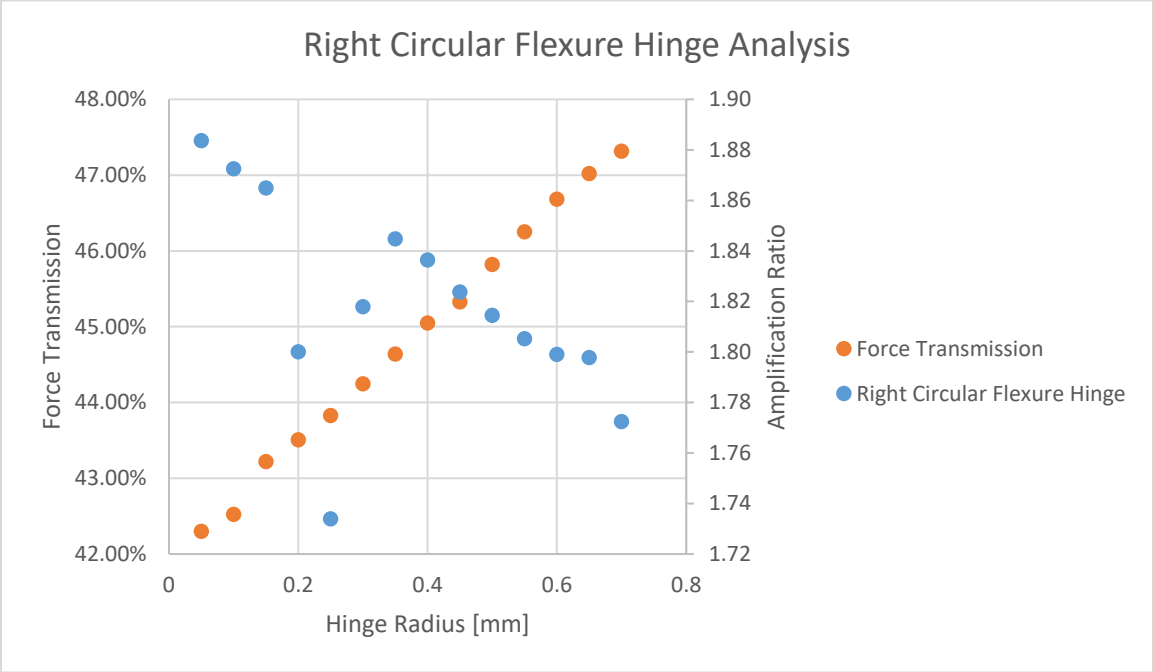

Figure 25: Right Circular Flexure Hinge Analysis

The data demonstrates a steady increase in force transmission as the hinge radius increases. Conversely, amplification ratio steadily decreases as radius increases and the thickness at the central axis of the flexure hinge decreases (with a peculiar dip between the 0.2 and 0.3 mm radius hinges). This shows that a thicker hinge transmits more force in total. Again, AR and FT proved to be inversely correlated and so the parameter AR/FD was plotted to analyze the optimal combination of the two parameters. Figure 26 exhibits amplification ratio over force dissipation.

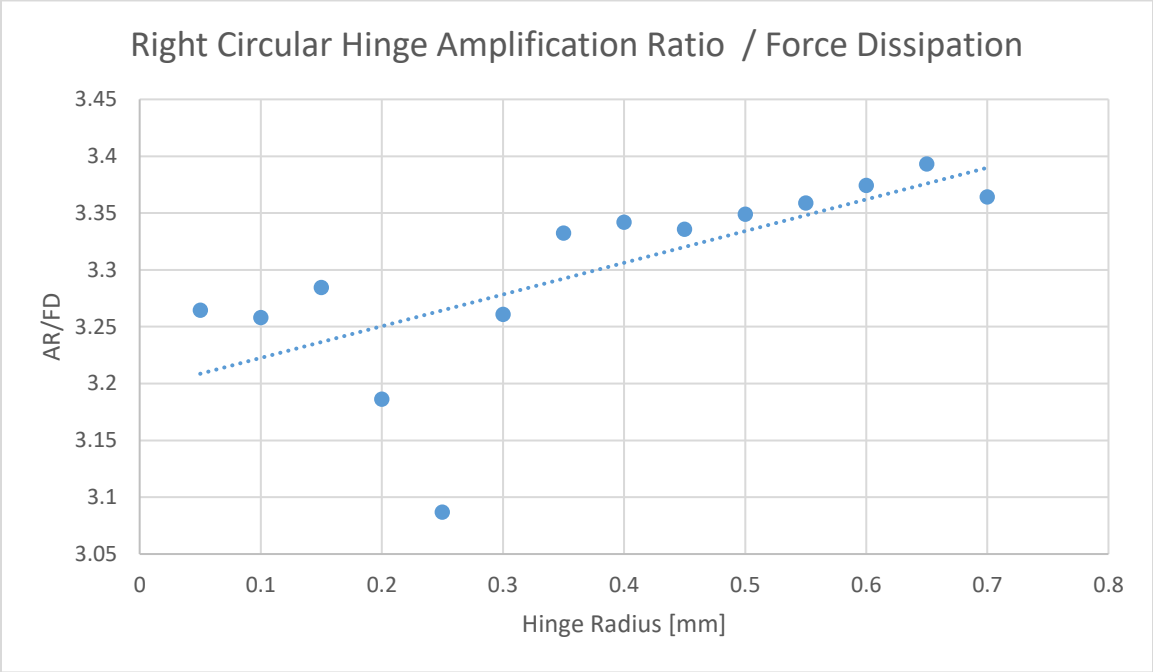

Figure 26: Right Circular Hinge Amplification Ratio / Force Dissipation

The AR/FD analysis demonstrates an approximately linear rising trend in the two equally weighted parameters as hinge radius increases (and central axis hinge thickness decreases). The peak performance of a right circular hinge at the lever amplifying mechanism demonstrates an AR/FD of around 3.4 before the hinge becomes too thin and subsequent stress exceeds the endurance limit of titanium. This analysis is to be compared with elliptic flexure hinges to determine the appropriate choice for this portion of the design.

4.4.2. Elliptical Flexure Hinge

The analysis of the elliptical flexure hinge was very similar to the right circular hinge analysis: parameters of the hinge were varied and FEA demonstrated the response of amplification ratio, force transmission, and Von Mises stress at the central hinge axis. However, for an elliptical hinge there are two input parameters: the two radii of the ellipse. In this study they are referred to as the length *l* of the ellipse and the thickness *t* of the hinge, as pictured in Figure 27. Since there were two input parameters, a Taguchi Array was used to determine the optimal combination of hinge thickness and length. The orthogonal array is included in Appendix D, but the summarized/averaged array is Table 3.

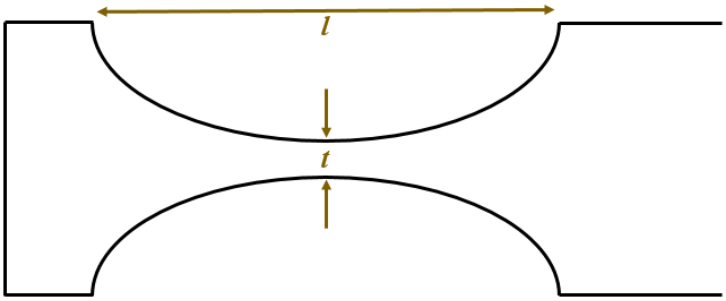

Figure 27: Elliptical Flexure Hinge Dimensional Parameters

Table 3: Elliptical Flexure Hinge Taguchi Analysis

Thickness [mm]	AR Average	FT Average	AR/FD Average
0.3	1.65	53.16%	3.52
0.5	1.15	53.00%	3.48
0.7	1.19	52.62%	3.50
0.9	1.15	52.46%	3.52
1.1	1.35	52.21%	3.51
1.3	1.38	51.92%	3.51
Coefficient Variation	0.134	0.008	0.004
Length [mm]			
1	1.68	51.77%	3.49
2	1.67	52.11%	3.50
3	1.68	52.12%	3.50
4	1.65	53.09%	3.53
5	1.65	53.21%	3.52
Coefficient Variation	0.009	0.011	0.004

The Taguchi Analysis demonstrates a strong inverse correlation between central hinge thickness and amplification ratio, while force transmission is much less affected by thickness with a coefficient of variation of 0.008. For this reason, thickness should be minimized without regard to its effect on force transmission. In turn, amplification ratio and force transmission seem to be about equally affected by the length of the hinge. A length of 4 mm demonstrates the highest AR/FD value. So, the optimal elliptical flexure hinge at the lever of the MDA proves to be 4 mm in length and 0.3 mm in thickness.

4.4.3. Lever Flexure Hinge Comparative Analysis

After the determination of the optimal right circular and elliptical flexure hinges for the lever of the MDA, the two choices were compared in order to make a final design decision. The comparative analysis measured a 0.7 mm radius right circular hinge against a 4 mm long, 0.3 mm thick elliptical flexure hinge on the basis of AR/FD calculated via FEA. The optimal right circular hinge exhibited an AR/FD value of about 3.4. The corresponding elliptical hinge demonstrated a value of about 3.6. In conclusion, the elliptical flexure hinge with the aforementioned thickness and length dimensions is the proper design choice for the rotation of the flexing lever amplifying mechanism.

4.5. Buckling Analysis

The entire mechanical displacement amplifier consists of two displacement mechanisms working in conjunction. The previous portion of this chapter discussed the parameters associated with the levers. The levers, however, transmit force to a bridge mechanism or buckling beam which must be modelled, analyzed, and optimized. This section is a comparative analysis of a bridge mechanism and a buckling beam. Various parameters associated with both types displacement mechanism will be varied to determine the essential outputs, and a comparative choice will be made based on total amplification ratio. In this section, force transmission as an output parameter is not considered, as the bridge is the final displacement mechanism. As long as the force is great enough to overcome the inertia of the magnet and electromagnetic damping of

the coil, it is sufficient. For this reason, the essential output parameters in this portion of the study will be amplification ratio and maximum Von Mises stress.

4.5.1. Bridge Mechanism

The bridge mechanism operates on the Pythagorean displacement amplification principle discussed in the literature review. Where it rotates, it utilizes double flexure hinges due to their low stiffness and reasonable precision. The input parameters examined in the bridge mechanism model were length *l* and thickness *t* of the flexure hinges as illustrated in Figure 28. Fillet radius was kept at 5% of the length of the hinge, according to the study conducted by Wei and King discussed in the literature review. Furthermore, the initial slant angle of the bridge α is to be varied. The outputs were amplification ratio considering the initial displacement to the lever, and max Von Mises stress in the hinges. Since there are three varying parameters, a non-orthogonal Taguchi Array was constructed. The full data is presented in Appendix E, and the Taguchi Analysis is included in Table 4.

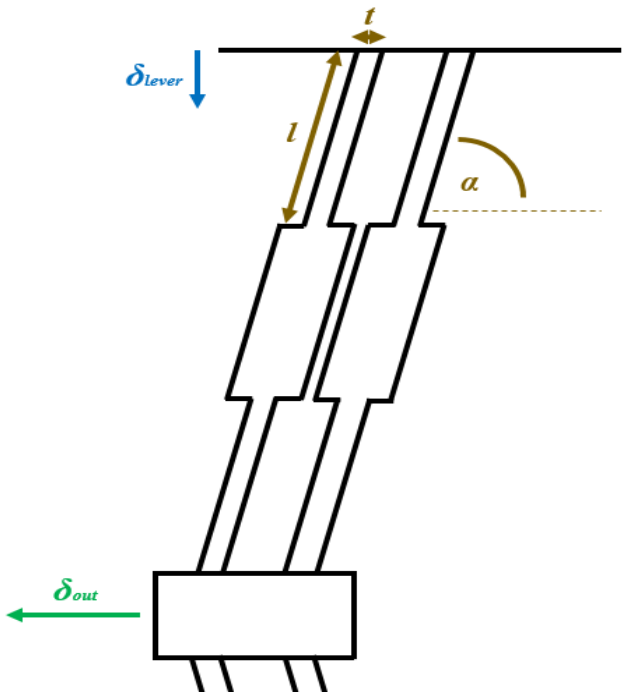

Figure 28: Double Corner-Filleted Flexure Hinge Bridge Mechanism

Table 4: Bridge Mechanism Double-Flexure Hinge Taguchi Analysis

Thickness [mm]	AR Average	Max VM Stress Average
0.2	11.77	379.65
0.3	10.79	401.08
0.4	9.47	377.53
0.5	7.73	342.68
Coefficient Variation	0.186	0.064
Length [mm]		
2	8.77	456.43
3	10.56	374.58
4	9.78	333.80
5	10.66	336.13
Coefficient Variation	0.086	0.132
Angle [°]		
85	13.39	417.93
82.5	10.61	418.98
80	8.71	336.03
78.5	7.06	328.00
Coefficient Variation	0.247	0.125

The maximum Von Mises stress averages are less important as long as the stress is below the 500 MPa endurance limit for hot isostatically pressed titanium. However, it is useful to generally keep in mind how the parameters are affecting the stress in the hinge.

According to the coefficients of variation, initial angle is the parameter that most strongly impacts amplification ratio. Smaller initial angles result in greater amplification, which makes sense considering the fundamental equations governing Pythagorean displacement amplification discussed in the literature review. Initial angle should be minimized to optimally amplify displacement; however, hinge stress also possesses a strong correlation with angle. Smaller

angles exert greater stresses on the hinges, so angle should be reduced just enough to maintain a max stress under the material's endurance limit.

Hinge thickness is the second most impactful parameter towards amplification ratio. Thinner hinges are less stiff and thus induce greater gain; the same issue with increased stress exists for a reduction of hinge thickness. The least significant parameter with regards to amplification ratio is hinge length. Hinge length, however, is the most significant parameter with regards to stress in the hinge. For this reason, the length of the hinge should be large in order to minimize stress, since the effect on amplification ratio is basically negligible.

Summarily, for the construction of double corner-filleted flexure hinges in an amplifying bridge mechanism, initial angle should be minimized, thickness should be minimized, and length should be increased to the point at which the max stress is just under the endurance limit. Next, a buckling beam will be considered.

4.5.2. Buckling Beam

The buckling beam that was modelled in this section adheres to all of the rules of buckling beams discussed in the literature review. It is a flat piece of titanium alloy, bounded at its ends, subjected to initial arcuate bending in order to reduce the critical buckling force and enforce buckling in only one direction.

The varying parameters in this study were the thickness and width of the beam as well as its initial bending angle. Considering an analysis of three parameters, a Taguchi Array was

constructed. The full data set is included in Appendix F, and the summarized analysis is shown in Table 5 below.

Table 5: Buckling Beam Taguchi Analysis

Thickness [mm]	AR Average	Max V.M. Stress Average
0.25	16.59	337.83
0.5	12.40	386.35
0.75	7.40	317.80
1	5.26	260.60
Coefficient Variation	0.42	0.14
Width [mm]		
4	10.87	361.05
6	8.69	310.33
8	13.22	365.13
10	8.88	266.08
Coefficient Variation	0.18	0.12
Angle [°]		
10	13.07	334.83
20	11.48	359.68
30	9.13	306.00
40	7.98	302.08
Coefficient Variation	0.19	0.07

The parameter that most strongly impacts amplification ratio is clearly the thickness of the beam. It should be minimized in order to maximize amplification ratio, at the risk of higher stresses in the beam. Width and initial angle proved to be similarly impactful on AR. Smaller initial angles result in larger amplification, as expected. The width of the beam exhibited erratic influence on the amplification ratio. However, it is strongly impactful upon the stress, with larger widths increasing the cross-section of the beam enough to reduce total stress at any given point. For this reason, 8 mm width was chosen for its high demonstrated gain and its reduction of total stress.

Summarily, a minimization of thickness and initial angle in combination with 8 mm width proves to be a buckling configuration that maximizes amplification ratio while maintaining reasonable stresses within the beam.

4.5.2. Bridge/Buckling Comparative Analysis

Following the determination of the optimal dimensions for the double flexure hinges of a bridge mechanism and for a buckling beam, the two options were compared for a final design decision. Across the entirety of the data sets for bridge and buckling beam, the buckling beam exhibited a 4.6% greater AR. In addition, the max modelled AR for the buckling beam was 28 compared to 17 for the bridge. Total stresses in the buckling beam were on average 15% lower than stresses within the bridge's flexure hinges. Considering the overall superiority of the buckling beam output parameters, this mechanism is the optimal design choice for the displacement amplification mechanism.

4.6. Conclusion

In conclusion, the proposed design for the mechanical displacement amplifier is based on a series of multi-variable FEA models and subsequent data analysis. The dimensions of each aspect of the design were thoroughly modelled at a range of values to determine the optimal values based on the essential parameters amplification ratio, force transmission, and maximum stress.

The results of this analysis are the following. The MDA is composed of an elliptical prism with a height that is 70% of its width. The outer shell is composed of a 1.5 mm thick titanium alloy. Force input is distributed across the entire cross-section of the lever. The levers are hinged at one end in order to amplify displacement on the other end. The hinge is 4 mm long elliptical flexure hinge with 0.3 mm thickness. The hinge inputs a force to a buckling beam of 8

mm width and 0.25 mm thickness. The following section discusses the experimental results of this design.

Chapter 5

Results

5.1. Mechanical Displacement Amplification

Following the process of using FEA to determine optimal values for every parameter within the MDA design, the final mechanical displacement amplifier design was determined. It is pictured in Figure 29.

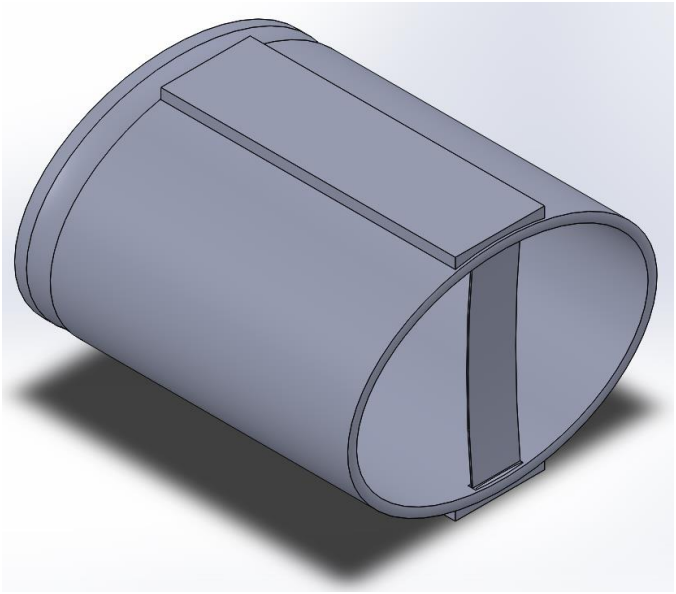

Figure 29: Final Mechanical Displacement Amplification Mechanism

In response to an 800 N force on the top and bottom, the MDA flexed an average of 5.02E-2 mm. Displacement at the center of the buckling beam was 1.44 mm. This is an amplification ratio of 28.68. As expected, this was a higher amplification ratio than in any of the previous FEA tests. The maximum Von Mises Stress during this test was 441 MPa, reasonably below the 500

MPa endurance limit for hot isostatically pressed titanium alloy. It should be mentioned that the amplification ratio can be significantly increased through a reduction in the width of the buckling beam. When the width was reduced from 8 mm to 3 mm, FEA demonstrated an AR of 31.29. However, the stress in the beam was about 780 MPa, significantly higher than the endurance limit. If this MDA is to be used over many cycles, the total stress must be lower than the endurance limit in order to ensure a long lifespan for the device. Figure 30 exhibits the MDA under flexure from the 800 N input force.

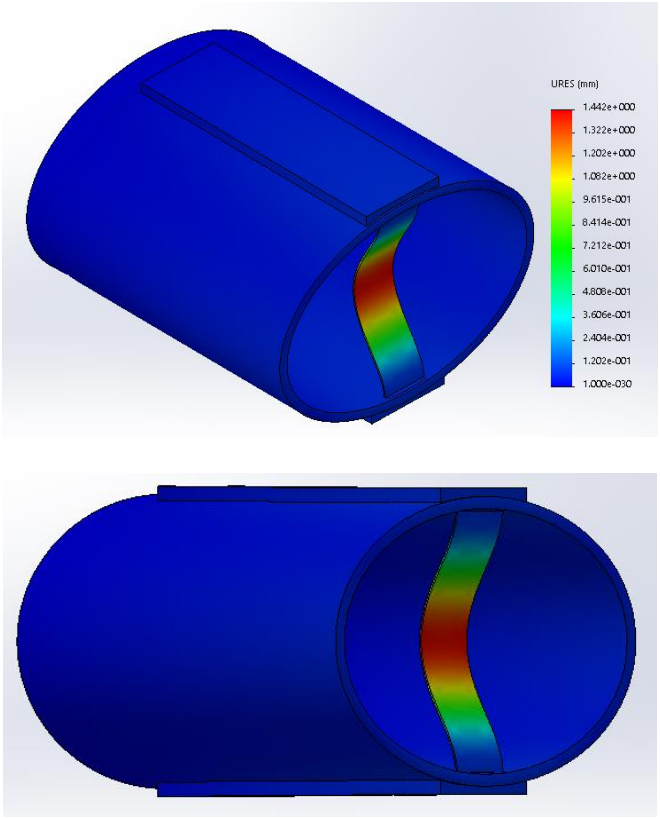

Figure 30: MDA Deformation

The mechanical displacement amplifier by itself is 5.0 cm x 3.6 cm x 5.2 cm. It has a total weight of 15.72 g and a volume of 15.7 cm^3. It vibrates at a natural frequency of 100 Hz.

5.2. Energy Generation

Mechanical displacement amplification devices have many applications; the design proposed in this thesis is targeted towards high force-input kinetic energy generation. While an amplification ratio of almost 30 within an elastic MDA is useful, the design must be conducive to energy generation to justify its viability. This section briefly discusses how the vibratory output displacement from the center of the buckling beam can be used to induce current in a coil. Figure 31 displays a more robust MDA design fitted with linear energy generation technology as well as connective mechanisms on the top and bottom. The flexing titanium frame is made transparent in the model, to show the internal energy generating components.

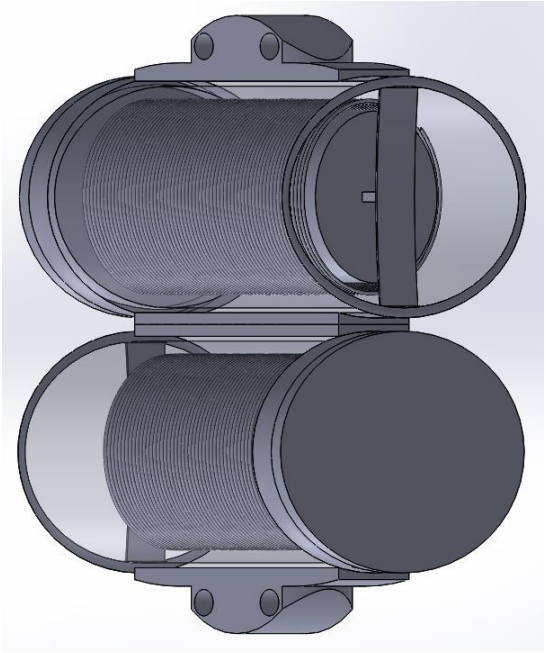

Figure 31: Energy Generation Potential Design

The potential kinetic energy harvester application for this MDA technology consists of two stacked MDA's in reverse orientation. The stacked design double's the energy output from

the MDA, and the reverse orientation eliminates the transverse displacement associated with a rotating lever mechanism, resulting in purely vertical displacement.

The energy generation system within the mechanical displacement amplifier consists of the following. Output displacement from the buckling beam is directed towards two neodymium magnets of 10-mm thickness and 26-mm diameter glued together and separated by a soft pole piece of 10-mm thickness. The coil is composed of a tenth-millimeter diameter copper wire wound 500 times within the internal cavity of the MDA. Although the electrical system is not expounded upon in this paper, a transformer and battery would be housed in the back portion of the IH.

The full energy harvester weights 81 g and occupies a volume of 68.9 cm^3. It vibrates at a resonance frequency of 2.82 Hz. This is a significant reduction from the original MDA; the reduction in frequency is due to the weight of the magnets attached to the buckling beam. A more thorough quantitative analysis of the energy generation application for the MDA requires an in-depth electromagnetic analysis; this thesis focuses on the mechanical displacement amplification principles of this design. However, it is useful to examine how this mechanical displacement amplification technology might be utilized for the purpose of ambient kinetic energy harvesting.

Chapter 6

Conclusions and Future Work

6.1. Findings

The goal of this research was to propose a novel, compliant, small-scale mechanical displacement amplification device tailored for high-force input ambient kinetic energy harvesting. While a more thorough analysis of energy-generation systems must take place, the mechanical systems demonstrate large amplification and force transmission in a durable, compact, elastic design.

The device elastically deforms under a uniform force input of 800 N and directs said deformation through a systems of flexing titanium sheet levers to a buckling beam. At its center, the buckling beam demonstrates an amplification ratio of 28.68 compared to the input displacement. In order to optimize each individual parameter of the design including force input, frame shape, flexure hinges, and the buckling beam, a comprehensive Finite Element Analysis was carried out for a series of dimensional parameters to illustrate how each variable impacted amplification ratio, force transmission, and maximum stress. The final MDA design weighed about 15.72 g and vibrated at a resonance frequency of 100.2 Hz. The force transmission at the center of the buckling beam was measured to be 2.44%.

6.2. Limitations and Next Steps

The primary limitation in the development of the mechanical displacement amplification device was lack of real-world experimental testing. The complex internal design of the MDA necessitates additive manufacturing processes, and the nature of the flexure hinges requires titanium alloy materials. Additive manufacturing using titanium was not financially viable considering the scope of this thesis.

Furthermore, micromechanical displacement amplification is always a means to an end, whether that be piezo-actuation, or energy harvesting, tactile displays, etc. This design in its elasticity and shape and dimensional characteristics is tailored towards energy generation via linear electromagnetic generation. An analysis of linear electromagnetic energy generation should take place to determine its compatibility with this MDA design. If it is determined that small scale linear electromagnetic generation is viable, the MDA proposed herein should be fitted with such energy generation technology and tailored for the optimization of power output. If this is done, then the mechanical displacement amplification design expounded upon in this thesis would have practical significance for many applications such as shoe soles, robotics, and prosthetics.

Appendix A

Input Force Data

Run	Area Percentage	*Disp_In [mm]*	*Disp_Out [mm]*	**AR**	**FT**	**AR/FD**
1	10%	6.22E-03	5.25E-03	0.84	N/A	N/A
2	20%	7.73E-03	6.52E-03	0.84	N/A	N/A
3	30%	7.03E-03	9.37E-03	1.33	16.19%	1.588939
4	40%	7.76E-03	1.38E-02	1.78	19.98%	2.228074
5	50%	8.62E-03	1.35E-02	1.56	24.28%	2.065035
6	60%	9.58E-03	1.55E-02	1.62	28.29%	2.25845
7	70%	1.07E-02	1.76E-02	1.65	35.04%	2.538803
8	80%	1.18E-02	1.96E-02	1.66	41.64%	2.84233
9	90%	1.40E-02	2.16E-02	1.54	47.90%	2.959339
10	95%	1.47E-02	2.23E-02	1.52	49.98%	3.043681

Appendix B

Frame Shape Taguchi Array

Run	**Height-Width Ratio**	**Thickness [mm]**	*Disp_In [mm]*	*Disp_Out [mm]*	**AR**	**FT**	**AR/FD**	*l [mm]*	*Theoretical Disp_Out [mm]*	**Theoretical AR**	**Theoretical AR/FD**
1	50.0%	4.5	8.87E-03	1.54E-02	1.73	44.05%	3.10	13.45	9.32E-02	10.50	18.76
2	55%	4.5	8.87E-03	1.50E-02	1.70	44.61%	3.06	14.80	9.14E-02	10.30	18.60
3	60%	4.5	8.81E-03	1.47E-02	1.67	45.12%	3.05	16.14	8.97E-02	10.18	18.54
4	65%	4.5	8.67E-03	1.44E-02	1.66	45.64%	3.05	17.49	8.76E-02	10.10	18.58
5	70%	4.5	8.52E-03	1.39E-02	1.63	46.25%	3.04	18.83	8.50E-02	9.97	18.56
6	75%	4.5	8.34E-03	1.35E-02	1.62	46.53%	3.04	20.18	8.28E-02	9.93	18.57
7	80%	4.5	8.17E-03	1.31E-02	1.61	46.69%	3.01	21.52	8.04E-02	9.84	18.46
8	85%	4.5	7.95E-03	1.27E-02	1.60	46.71%	3.01	22.87	7.81E-02	9.82	18.43
9	90%	4.5	7.72E-03	1.23E-02	1.59	46.75%	2.99	24.21	7.55E-02	9.77	18.35
10	95%	4.5	7.55E-03	1.19E-02	1.58	46.60%	2.96	25.56	7.33E-02	9.72	18.20
11	100%	4.5	7.35E-03	1.16E-02	1.57	46.58%	2.95	26.90	7.11E-02	9.67	18.11
12	50%	3.0	2.35E-02	4.15E-02	1.76	47.91%	3.38	13.45	2.43E-01	10.32	19.81
13	55%	3.0	2.29E-02	3.97E-02	1.74	47.97%	3.34	14.80	2.34E-01	10.23	19.67
14	60%	3.0	2.21E-02	3.81E-02	1.72	47.90%	3.31	16.14	2.26E-01	10.22	19.62
15	65%	3.0	2.13E-02	3.61E-02	1.70	48.11%	3.27	17.49	2.15E-01	10.13	19.52
16	70%	3.0	2.02E-02	3.43E-02	1.70	48.14%	3.27	18.83	2.05E-01	10.16	19.59
17	75%	3.0	1.93E-02	3.25E-02	1.68	48.07%	3.23	20.18	1.95E-01	10.09	19.43
18	80%	3.0	1.84E-02	3.08E-02	1.67	48.01%	3.21	21.52	1.86E-01	10.07	19.38
19	85%	3.0	1.76E-02	2.90E-02	1.65	47.82%	3.17	22.87	1.76E-01	9.99	19.15
20	90%	3.0	1.66E-02	2.74E-02	1.65	47.81%	3.16	24.21	1.66E-01	10.01	19.17
21	95%	3.0	1.59E-02	2.61E-02	1.64	47.69%	3.14	25.56	1.58E-01	9.98	19.08
22	100%	3.0	1.51E-02	2.45E-02	1.63	47.52%	3.10	26.90	1.49E-01	9.90	18.86
23	50%	1.5	8.88E-02	1.63E-01	1.84	49.39%	3.64	13.45	8.41E-01	9.48	18.73
24	55%	1.5	7.95E-02	1.45E-01	1.82	48.96%	3.57	14.80	7.68E-01	9.66	18.93
25	60%	1.5	7.18E-02	1.30E-01	1.81	48.65%	3.53	16.14	7.06E-01	9.82	19.13
26	65%	1.5	6.49E-02	1.16E-01	1.79	47.93%	3.44	17.49	6.44E-01	9.93	19.06
27	70%	1.5	5.86E-02	1.05E-01	1.78	47.72%	3.41	18.83	5.88E-01	10.04	19.20
28	75%	1.5	5.36E-02	9.48E-02	1.77	47.77%	3.38	20.18	5.40E-01	10.08	19.30
29	80%	1.5	4.89E-02	8.55E-02	1.75	47.54%	3.33	21.52	4.93E-01	10.07	19.20
30	85%	1.5	4.52E-02	7.81E-02	1.73	47.15%	3.27	22.87	4.55E-01	10.07	19.05
31	90%	1.5	4.26E-02	7.31E-02	1.71	46.65%	3.21	24.21	4.28E-01	10.05	18.84
32	95%	1.5	3.95E-02	6.71E-02	1.70	46.09%	3.15	25.56	3.96E-01	10.02	18.59

33	100%	1.5	3.78E-02	6.37E-02	1.69	45.97%	3.12	26.90	3.77E-01	10.00	18.50

Appendix C

Right Circular Flexure Hinge Data

Run	Radius [mm]	Thickness [mm]	*Disp_In [mm]*	*Disp_Out [mm]*	**AR**	**FT**	**Von Mises Stress [Mpa]**	**AR/FD**
1	0.05	1.4	4.59E-02	8.65E-02	1.88	42.30%	234.2	3.26
2	0.1	1.3	4.68E-02	8.77E-02	1.87	42.52%	212	3.26
3	0.15	1.2	4.77E-02	8.89E-02	1.86	43.22%	191.4	3.28
4	0.2	1.1	6.48E-02	1.08E-01	1.67	43.51%	206.1	2.96
5	0.25	1	5.68E-02	9.85E-02	1.73	43.83%	228.5	3.09
6	0.3	0.9	4.89E-02	8.89E-02	1.82	44.25%	235.9	3.26
7	0.35	0.8	4.98E-02	9.19E-02	1.84	44.64%	280.8	3.33
8	0.4	0.7	5.09E-02	9.35E-02	1.84	45.05%	234.3	3.34
9	0.45	0.6	5.23E-02	9.54E-02	1.82	45.33%	261.4	3.34
10	0.5	0.5	5.35E-02	9.71E-02	1.81	45.82%	267.4	3.35
11	0.55	0.4	5.50E-02	9.94E-02	1.81	46.25%	305.0	3.36
12	0.6	0.3	5.74E-02	1.03E-01	1.80	46.68%	355.7	3.37
13	0.65	0.2	5.99E-02	1.08E-01	1.80	47.02%	374.6	3.39
14	0.7	0.1	6.37E-02	1.13E-01	1.77	47.32%	476.3	3.36

Appendix D

Elliptical Flexure Hinge Taguchi Array

Run	Thickness [mm]	Length [mm]	*Disp _In [mm]*	*Disp_Out [mm]*	**AR**	**FT**	**Von Mises Stress [Mpa]**	**AR/FD**
1	1.3	5	6.55E-02	1.09E-01	1.66	52.59%	189.1	3.50
2	1.1	5	6.73E-02	1.11E-01	1.65	52.81%	192.1	3.51
3	0.9	5	6.98E-02	1.15E-01	1.65	53.01%	200.1	3.51
4	0.7	5	7.28E-02	1.20E-01	1.64	53.27%	209.5	3.52
5	0.5	5	7.72E-02	1.26E-01	1.64	53.63%	228.1	3.53
6	0.3	5	8.19E-02	1.33E-01	1.63	53.96%	242.1	3.54
7	1.3	4	6.52E-02	1.08E-01	1.66	52.07%	189.8	3.46
8	1.1	4	6.68E-02	1.11E-01	1.66	52.80%	190.9	3.51
9	0.9	4	6.69E-02	1.14E-01	1.70	52.98%	196.5	3.61
10	0.7	4	7.14E-02	1.18E-01	1.64	53.34%	208.5	3.52
11	0.5	4	7.53E-02	1.23E-01	1.64	53.53%	222.6	3.52
12	0.3	4	7.91E-02	1.29E-01	1.63	53.85%	240.6	3.54
13	1.3	3	6.32E-02	1.07E-01	1.69	51.67%	175	3.50
14	1.1	3	6.35E-02	1.07E-01	1.68	51.87%	180.3	3.50
15	0.9	3	6.51E-02	1.09E-01	1.68	52.06%	182	3.50
16	0.7	3	6.68E-02	1.12E-01	1.67	52.36%	192.7	3.51
17	0.5	3	6.82E-02	1.14E-01	1.67	52.43%	195.9	3.51
18	0.3	3	6.83E-02	1.14E-01	1.67	52.36%	223.5	3.51
19	1.3	2	6.19E-02	1.05E-01	1.69	51.65%	178.2	3.49
20	1.1	2	6.29E-02	1.06E-01	1.68	51.87%	180.2	3.50
21	0.9	2	6.42E-02	1.08E-01	1.68	52.03%	184.3	3.50
22	0.7	2	6.57E-02	1.10E-01	1.67	52.22%	196.4	3.50
23	0.5	2	6.79E-02	1.13E-01	1.66	52.40%	222.9	3.49
24	0.3	2	6.93E-02	1.15E-01	1.66	52.49%	280.8	3.50
25	1.3	1	6.17E-02	1.04E-01	1.69	51.62%	173.6	3.49
26	1.1	1	6.24E-02	1.05E-01	1.68	51.70%	184.1	3.49
27	0.9	1	6.31E-02	1.06E-01	1.68	51.85%	484	3.49
28	0.7	1	6.40E-02	1.08E-01	1.68	51.90%	256.8	3.49
29	0.5	1	N/A	N/A	N/A	N/A	N/A	N/A
30	0.3	1	N/A	N/A	N/A	N/A	N/A	N/A

Appendix E

Bridge Double-Flexure Hinge Taguchi Array

Run	Thickness [mm]	Length [mm]	Angle	*Disp_In [mm]*	*Disp_Out [mm]*	**AR**	**Von Mises [Mpa]**
1	0.5	5	78.5	5.34E-02	3.55E-01	6.65	298.3
2	0.5	4	80	4.74E-02	3.67E-01	7.74	329.2
3	0.5	3	82.5	3.84E-02	3.31E-01	8.62	355.8
4	0.5	2	85	2.82E-02	2.24E-01	7.93	387.4
5	0.4	5	82.5	4.87E-02	5.07E-01	10.41	357.9
6	0.4	4	85	3.80E-02	4.70E-01	12.39	367.9
7	0.4	3	78.5	5.83E-02	4.06E-01	6.96	341.9
8	0.4	2	80	5.07E-02	4.11E-01	8.11	442.4
9	0.3	5	85	4.92E-02	7.65E-01	15.54	452.6
10	0.3	4	82.5	5.69E-02	6.54E-01	11.50	390.6
11	0.3	3	80	6.11E-02	5.47E-01	8.96	336.8
12	0.3	2	78.5	6.16E-02	4.42E-01	7.17	424.3
13	0.2	5	80	6.71E-02	6.72E-01	10.02	235.7
14	0.2	4	78.5	6.78E-02	5.07E-01	7.47	247.5
15	0.2	3	85	5.94E-02	1.05E+00	17.69	463.8
16	0.2	2	82.5	5.99E-02	7.12E-01	11.89	571.6

Appendix F

Buckling Beam Taguchi Array

Run	Thickness [mm]	Width [mm]	Angle [^{o}]	*Disp_In [mm]*	*Disp_Out [mm]*	**AR**	**Max Von Mises Stress [Mpa]**
1	0.5	4	10	3.67E-02	6.16E-01	16.80	444.5
2	0.5	6	20	4.55E-02	6.26E-01	13.74	446.5
3	0.5	8	30	5.15E-02	5.43E-01	10.56	360.5
4	0.5	10	40	5.62E-02	4.79E-01	8.53	293.9
5	1	4	20	2.94E-02	2.01E-01	6.82	343.4
6	1	6	10	2.17E-02	6.22E-02	2.87	186.1
7	1	8	40	3.45E-02	2.08E-01	6.02	286.2
8	1	10	30	2.59E-02	1.39E-01	5.34	226.7
9	0.25	4	30	6.69E-02	7.90E-01	11.80	248
10	0.25	6	40	6.77E-02	6.32E-01	9.33	219.9
11	0.25	8	10	4.97E-02	1.40E+00	28.10	524.2
12	0.25	10	20	6.04E-02	1.04E+00	17.14	359.2
13	0.75	4	40	5.42E-02	4.36E-01	8.05	408.3
14	0.75	6	30	4.13E-02	3.65E-01	8.83	388.8
15	0.75	8	20	2.89E-02	2.37E-01	8.21	289.6
16	0.75	10	10	2.11E-02	9.56E-02	4.53	184.5

BIBLIOGRAPHY

[1] Hu, Youfan, et al. *Hybridizing Triboelectrification and Electromagnetic Induction Effects for High-Efficient Mechanical Energy Harvesting*. ACS Nano, 2014. **8**(7): p. 7442-7450.

[2] Lobontiu, Nicolae, and Ephraim Garcia. *Analytical Model of Displacement Amplification and Stiffness Optimization for a Class of Flexure-Based Compliant Mechanisms*. Computers and Structures, 2003. **81**: p. 2797-2810.

[3] Ouyang, P. R., et al. *A New Compliant Mechanical Amplifier Based on a Symmetric Five-Bar Topology*. ASME, 2008. **130**: p. 2-10.

[4] Ma, Hong-Wen, et al. *Analysis of the Displacement Amplification Ratio of the Bridge-Type Flexure Hinge*. Sensors and Actuators A: Physical, 2006. **132**: p. 730-736.

[5] Newnham, R. E., et al. *Flextensional 'Moonie' Actuators.* Ultrasonics Symposium, 1993: p. 509-513.

[6] Lobontiu, Nicolae. *Compliant Mechanisms.* Compliant Mechanisms, 2003: p. 11-24.

[7] King, T., and W. Xu. *The Design and Characteristics of Piezomotors using Flexure-Hinged Displacement Amplifiers.* Robotics and Autonomous Systems, 1996: p. 189-197.

[8] Xu, Wei, and Tim King. *Flexure Hinges for Piezoactuator Displacement Amplifiers: Flexibility, Accuracy, and Stress Considerations*. Precision Engineering, 1996. **19**(10): p. 4-10.

[9] Saif, and Macdonald. *Measurement of Forces and Spring Constants of Microinstruments.* Review of Scientific Instruments, 1997. **69**(3): p. 1410-1422.

[10] Yoon, Hwak-Sik. *A Millimeter-Stroke Piezoelectric Hybrid Actuator using Hydraulic Displacement Amplification Mechanism*. IEEE ISIE, 2006: p. 2809-2813.

[11] Ninomiya, T., et al. *MEMS-Based Hydraulic Displacement Amplification Mechanism with Completely Encapsulated Liquid*. Sensors and Actuators A: Physical, 2003. **3**(14): p. 277-282.

[12] Paros, J. M., and L. Weisbord. *How to Design Flexure Hinges*. Machine Design, 1965, **37**: p. 151-156.

[13] Furukawa, Eiichi, et al. *A Magnifying Mechanism for Use on Piezo-Driven Mechanisms.* Journal of the Japan Society for Precision Engineering, 1991. **57**(8): p. 1363-1368.

[14] Hrabe, Nikolas, et al. *Fatigue Properties of a Titanium Alloy (Ti-6Al-4V) Fabricated Via Electron Beam Melting (EBM): Effects of Internal Defects and Residual Stress.* International Journal of Fatigue, 2017. **94**: p. 202-210.

[15] Briscoe, Joe, and Steve Dunn. *Piezoelectricity and Ferroelectricity*. Nanostructured Piezoelectric Energy Harvesters, 2014, p. 3-16.

[16] Xu, Shiyou, et al. *Flexible Piezoelectric PMN−PT Nanowire-Based Nanocomposite and Device.* NANO letters, 2013. **13**(6): p. 2393-2398.

[17] Duffy, M., and D. Carroll. *Electromagnetic Generators for Power Harvesting*. IEEE 35th Annual Power Electronics Specialists Conference, 2004. **3**: p. 2075-2081.

[18] Bouendeu, Emmanuel, et al. *A Low-Cost Electromagnetic Generator for Vibration Energy Harvesting*. IEEE Sensors Journal, 2011. **11**(1): p. 107-113.

[19] Saha, C. R., et al. *Electromagnetic Generator for Harvesting Energy from Human Motion*. Actuators A: Physical, 2008. **147**: p. 248-253.

[20] Kong, Ling Bing, et al. *Piezoelectric Effect*. Waste Energy Harvesting, 2014. **24**: p. 19-42.

[21] Dorsch, P., et al. *Towards a Miniaturized, Impulse-Excited Piezoelectric Energy Harvesting Device.* Procedia Engineering, 2015. **120**: p. 1032-1036.

Academic Vita

Education

The Pennsylvania State University, Schreyer Honors College — **University Park, PA**
Bachelor of Science with Honors in Mechanical Engineering — Class of May 2018

University of Freiburg — **Freiburg, Germany**
Liberal Arts — *January 2016 – June 2016*

- Experienced a liberal arts education within the context of the German education system
- Attended classes with German students on the subjects of religion, African authoritarianism, ethnic diversity, and ancient trade systems
- Lived within and learned about the unique and rapidly changing 21st century German culture

Professional Experience

Procter & Gamble — **Mehoopany, PA**
Process Manufacturing Intern — *June 2017 – August 2017*

- Identified an opportunity to rewrite the logic of a paper winder for $654,000 average annual savings
- Implemented a programming change in a paper winder for $4,500 annual savings
- Coded a program in Visual Basic to pull line data and auto-populate a statistics board in the team's daily morning meeting
- Developed and had fabricated a system of color-coded carts for the storage and organization of core plugs on the floor
- Designed, built, and implemented a pulley mechanism for lifting a 500 pound dust hood
- Conducted predictive maintenance on a case-packer through the development of an uptime inspection route

T3 Solutions — **Freiburg, Germany**
Combined Heat and Power Intern — *June 2016 – August 2016*

- Serviced 6 combined heat and power (CHP) units throughout the Black Forest region of Germany
- Analyzed system-level schematics for CHP units
- Conducted load and material strength calculations for the design plans of a new sunshade product
- Gained firsthand experience in the management and working style of a German engineering company

GHD Engineering Services — **San Francisco, CA**
HVAC Intern — *June 2015- August 2015*

- Reviewed building codes and federal regulations, applying them to specific project designs
- Surveyed field operations and conducted relevant measurements on project sites
- Calculated building specifications in order to size equipment
- Contacted HVAC vendors to determine appropriate equipment for designs

Leadership

USSF Soccer Referee — *March 2010 – Present*

- Established authority on a soccer field of hundreds of players, coaches, and parents

YMCA Camp Counselor — *June 2014 – August 2014*

- Led, controlled, and developed lesson plans for a group of 10-15 12-year-olds through summer camp

Honors and Awards

Dean's List; *Fall 2014 - Fall 2017*
Provost's Award for Academic Excellence; *2014*
William A. Schreyer Scholarship; *2014*
Brandon M. Boger Memorial Scholarship; *2014*

Skills

Matlab	Public Speaking
Visual Basic	MSO
Javascript	Excel
Solidworks	Revit